Master's Thesis

Detectability of ω meson mass modification with pole dropping and/or broadening scenarios

Hiroshima University
Graduate School of Advanced Science and Engineering
Quark Physics Laboratory
M202476

Keisuke Tomohiro

Supervisor: Prof. Kenta Shigaki
Vice Supervisor: Assoc. Prof. Yorito Yamaguchi
Vice Supervisor: Prof. Chikako Moriyoshi

January 31, 2023

Abstract

物理学の標準模型の指導原理の一つに、ゲージ原理がある。これによりすべての素粒子は質量が 0 であることを要求されるが、実際にはヒッグス機構を通して素粒子に質量が与えられる。しかし、陽子などのハドロンはヒッグス機構によってその質量の 1%程度しか獲得せず、物質質量の起源には未だ謎が残る。残りの大部分の質量起源と目す「カイラル対称性の自発的破れ」はその度合いを温度で変化させる。このために高温環境下でハドロンの質量状態変化を検出することは、ハドロンの質量起源に対し大きな示唆を与える。国際共同実験 ALICE におけるこれの検出を見据え、事前の検出可能性評価を行なったことがこの研究である。

本研究は、CERN 研究所 LHC 加速器を用いて実施する ALICE 実験において、カイラル相転移に伴うω中間子の質量状態変化について、コンピュータシミュレーションを用いてその検出可能性を示す。カイラル相転移とは物質の質量状態を変化させると考えられる相転移であり、LHC 加速器では重イオン衝突によりカイラル相転移に十分な高温物質を生成できる。ω中間子は質量状態変化のある高温物質内で崩壊できる程度に寿命が短いことに加え、強い相互作用をせず崩壊時点での粒子の情報を検出器まで保持できるμ粒子対に崩壊するモードが存在するため、本研究ではこの粒子に着目した。ALICE 実験では質量状態変化の検出には至っていないが、2022 年より稼働中の LHC 第三期運転では、検出器の前方領域にμ粒子飛跡測定のための新規検出器を導入した。これにより前方μ粒子の質量分解能の向上と背景事象のより高精度な見積もりが見込め、これまで不可能であった前方領域での高精度なμ粒子対不変質量測定が可能となる。さらに低横運動量の粒子は高温物質中に留まる時間が長く、質量状態変化のある状態でμ粒子に崩壊する確率が高いが、この低横運動量μ粒子を同定しやすい検出領域がこの前方領域である。よって、カイラル相転移に伴う質量状態変化の検出に向けては、前方領域での 検出可能性を評価することが重要となる。本論文では、第三期運転でのω中間子質量状態変化検出を見据え、すでに完了している LHC 第二期運転で収集したデータを元に作成した前方領域におけるμ粒子対の不変質量分布を解析し、ω中間子質量状態変化の検出可能性の定量的な評価を行った。先行研究では、中心値の変移を伴うω中間子の質量状態変化について検出可能性の評価を行なっている。これはカイラル相転移によりω中間子が質量を獲得すると考えられることから、ω中間子の質量が単純に軽くなるように仮定したシナリオである。本研究ではその先行研究を基礎として、幅の変移を伴うω中間子質量状態変化を行なった。これは NA60 実験が、ω中間子と同様のベクトル中間子であるρ中間子の質量幅変化を支持する結果を出していることから可能性のある質量状態変化であると考え仮定したシナリオである。さらに、中心値と幅が同時に変移するシナリオに基づいた検出可能性の評価も行った。これらシナリオ毎の結果を踏まえ、ALICE 実験におけるω中間子質量状態変化の検出可能性について考察する。

Contents

List of Figures

1 Introduction

Physics is a science field that quest the universal law of nature. In particular, elementary particle physics is a field that explores the question, "What is this world made of?" Currently, the question has been replaced by understanding the most fundamental elements and interactions existing in nature. The summary of elementary particle physics is the Standard Model. The Standard Model is a highly successful model that describes almost all high-energy physical phenomena without contradictions. This mainly consists of Quantum electrodynamics (QED) and Quantum chromodynamics (QCD). Both of these are gauge theories, which are based on the gauge principle [Section:2.1]. The gauge principle requires the mass of elementary particles to be zero. This seems to be factually incorrect, by being discovered the Higgs particle in 2012[8][9], even the problem has been gone. However, there is a still mystery about mass. Hadrons, such as protons or neutrons, gain only part of their mass from the Higgs field. The rest of the mass origin remains as unknown.

High-energy physics is an experimental field to investigate particle physics. Accelerators are the means to approach high-energy regions. The Large Hadron Collider, LHC[10][11][12], is the largest accelerator in the world. Giant accelerators are microscopes, because the higher energy, the smaller scale will be seen. Now the LHC can reach the micro level of elementary particles, such as quarks and gluon. Moreover, the LHC can deconstruct hadrons into quarks and gluons with high energy. This is called deconfinement. Besides, the deconfinement state is called quark-gluon plasma, QGP, which has been discovered at RHIC[13]. This had existed only at the beginning of the universe. Now particle accelerator is the unique means to approach quark-gluon plasma or the beginning of the universe. Furthermore, chiral symmetry may restore partially in this high-energy region. This means there may be a possibility that hadron mass is different from it in a vacuum.

Until now, some experiments have tried to discover mass modification by chiral restoration in high-energy regions[14]. In particular, light vector mesons, ρ, ω and ϕ, are expected to change their mass in high-energy region, this is because their of light masses and the decay mode to dilepton. Electron is a probe to survey the mass spectrum, but Dalitz decay brings many backgrounds. Thereby, mass modification has not been found. A Large Hadron Collider Experiment, ALICE[6][15], is one of such experiments. ALICE is implemented at a point of the LHC. The past runs of the LHC, Run 1 and Run 2 are already finished. However, mass modification by chiral symmetry restoration has not been found. From Run 3, which started last year, the ALICE detector installed Muon Forward Tracker, MFT[16]. Owning to this, ALICE can measure muon more precisely in the forward region. Another probe to survey the mass spectrum is muon. In addition, the forward region is suitable to search mass modification of low-mass vector meson because the forward particle is easier to decay in quark-gluon plasma. Due to this situation, the momentum for finding a mass modification in Run 3 at ALICE heightens.

In this study, detectability of ω meson mass modification is evaluated based on $\sqrt{s} = 13$ TeV pp collisions data collected in Run 2 in 2016 using ALICE detector at the LHC. A mass dropping, the mass modification way that the mean mass shifts to lighter, and a mass broadening, the mass modification way that the mass spectrum width broadens, are considered. Additionally, a mass modification way that the mass drops and broadens simultaneously is also considered.

This study is focused on low-mass vector meson mass modification analysis in Run 3 in Pb-Pb collisions at ALICE. The Pb-Pb collision is planned to run in November 2023. This study is worthwhile as a baseline assessment toward the analysis. Understanding of mass modification of hadrons leads to the origin of hadron mass.

2 Physics Background

The universe, which began with the hot fireball Big Bang, has gradually cooled down. It has undergone many phase transitions. And just as water "spontaneously breaks symmetry" when it becomes ice, the universe is thought to have reached its present state through repeated symmetry breaking since the Big Bang. Yoichiro Nambu's theory was the first to point out what happens with this "spontaneous symmetry breaking," and was awarded the Nobel Prize in 2008. Spontaneous symmetry breaking for chiral symmetry, which is the symmetry of quarks property called chirality, is thought to be the origin of most hadron mass. The related physics is described in this chapter.

2.1 Gauge principle

Gauge transformation is equivalent to changing the scale of a measure. It is to multiply a field by a complex number and change its phase. And the fact that the form does not change for the gauge transformation is called gauge symmetry. If it is invariant under different gauge transformations at each point in spacetime, in, particular, it has local gauge symmetry. For example, one can increase or decrease the value of the electromagnetic potential at each spacetime point, but the electric and magnetic fields will not change. And the form of Maxwell's equations does not change either. This means that Maxwell's electromagnetic theory has local gauge symmetry. Quantum electrodynamics (QED) theory and Quantum chromodynamics (QCD) theory are built on local gauge symmetry as a principle. Forces arising from gauge symmetries are mediated based on gauge particles. The gauge particles mediating the electromagnetic force are photons, gluons in the case of strong forces, and W and Z particles in the case of weak forces. As a consequence of imposing the gauge principle, the mass of a gauge particle must be zero. Photons and gluons have no mass within the measurement precision. However, in 1968, it was theoretically predicted that the weak boson has about 90 times the mass of the proton. In fact, it has been confirmed that W bosons and Z bosons have mass. This makes it impossible to construct a theory based on the gauge principle. The solution to this is spontaneous gauge symmetry breaking, called the Higgs mechanism, and in general, spontaneous symmetry breaking proposed by Yoichiro Nambu.

2.2 Spontaneously symmetry breaking

Spontaneous symmetry breaking is a theory presented by Yoichiro Nambu in 1961[17][18]. The Nanbu-Jona-Lasinio (NJL) model was the first to apply the idea of spontaneous symmetry to particle physics. Spontaneous symmetry breaking is a phenomenon that occurs in certain physical systems where a continuous symmetry of the underlying laws of the system is not reflected in the lowest-energy state of the system. The result is that the ground state is not symmetrical, even though the laws of the system possess that symmetry.

One of the key features of spontaneous symmetry breaking is that it can result in the formation of new particles with mass, even if the underlying laws of physics are symmetrical and do not contain any explicit mass terms. This is known as mass generation and occurs because the ground state of the system is not symmetrical, meaning that the fluctuations in the ground state can have non-zero expectation values. Another of the key features of spontaneous breaking is that it results in the formation of a Nambu-Goldstone (NG) boson, which is a massless particle that is associated with broken symmetry. The NG boson is a manifestation of broken symmetry, and its properties can be used to study the properties of the system and the underlying symmetries.

In particle physics, spontaneous symmetry breaking plays a central role in the Higgs mechanism, which is responsible for giving particles mass.

2.3 Higgs mechanism

Applying spontaneous symmetry breaking to gauge theory, gauge bosons can generate mass while preserving the gauge symmetry. This was proposed in 1964 by several independent studies[19][20][21], respectively. The theory is named after physicist Peter Higgs, who first proposed the idea. According to the Higgs mechanism, a scalar field called the Higgs field permeates all of space. This field has a non-zero expectation value in the ground state, meaning that it has a non-zero value even in the absence of any particles. The non-zero value of the Higgs field breaks the symmetries of the underlying laws of physics, leading to the generation of mass for some particles. The shape of the Higgs potential is a wine bottle or double-well potential, meaning it has a minimum value at a non-zero field strength, which corresponds to the non-zero mass of particles. The degrees of freedom to move around along the bottom of the wine bottle potential can be turned into a mass term of gauge bosons. This mechanism produces three vector particles with masses, W^+, W^- and Z^0 bosons, and a vector particle with no mass, photon. One scalar particle is the Higgs boson. Other particles also acquire mass by interacting with a field of energy that permeates the universe. This field is called the Higgs field, and particles that interact with it acquire mass by slowing down as they move through the field. The strength of the interaction between a particle and the Higgs field determines the particle's mass.

The Higgs mechanism was confirmed in 2012 when scientists at the Large Hadron Collider (LHC) at CERN in Geneva, Switzerland, discovered the Higgs boson[8][9]. The discovery of the Higgs boson confirmed the existence of the Higgs field and the validity of the Higgs mechanism.

2.4 Quantum chromodynamics

Quantum Chromodynamics (QCD) is the theory of the strong force, one of the four fundamental forces of nature. It describes the interactions between quarks and gluons, the particles that make up protons and neutrons, which

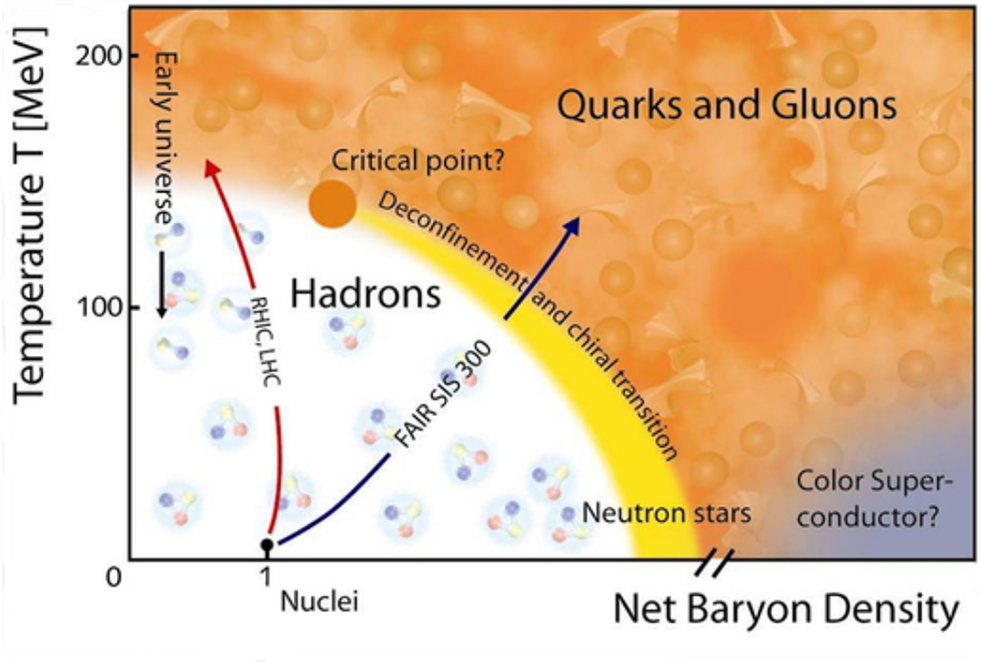

Figure 1: The QCD phase diagram, with a hadron phase of ordinary nuclear matter and a quark gluon plasma phase. [At zero matter (baryon) density the phase transition is established to be a smooth crossover, current research searches for a first order transition and a critical point at finite density.[1]

are the building blocks of atomic nuclei. QCD is a very successful theory, with predictions that have been confirmed by numerous experiments. It is also a key component of the standard model of particle physics, which describes the behavior of all known particles and their interactions. Some of the key properties of QCD are:
Confinement: Quarks are never found as isolated particles, but are always confined inside hadrons.
Asymptotic freedom: At high energies, quarks and gluons behave as free particles, while at low energies, they are tightly bound inside hadrons.
Non-abelian gauge theory: QCD is a non-abelian gauge theory.
Color charge: Quarks come in three different "colors", and the interactions between quarks are governed by the exchange of gluons, which carry the color charge.
Complexity: QCD is a highly complex theory, and its predictions can only be obtained through numerical simulations or approximate analytical methods.
Strong CP problem: QCD is believed to violate the CP symmetry, but the magnitude of this violation is not well understood and is known as the strong CP problem.

2.4.1 Quark confinement

Quark confinement is a phenomenon in particle physics where individual quarks cannot be observed as free particles. The strong interaction makes

it energetically unfavorable for a single quark to exist as a free particle. As a result, quarks are always found inside hadrons and attempts to isolate and observe a single quark have so far been unsuccessful. This is known as quark confinement. This is a key property of QCD. The exact mechanisms behind quark confinement are still not well understood and are an active area of research. Some theories suggest that the confinement is due to the formation of a type of theoretical object known as a flux tube between the quarks, while others propose that it is the result of the gluons' self-interactions. Despite the lack of a complete understanding, quark confinement has been experimentally confirmed and is considered a well-established concept in particle physics.

2.4.2 Spontaneous symmetry breaking of chiral symmetry

Chiral symmetry is a symmetry that relates the interactions of particles with left-handed and right-handed spin. In QCD, chiral symmetry is an approximate symmetry, which is broken by the strong force interactions between quarks and gluons. The breaking of chiral symmetry is responsible for the generation of masses for the light quarks and the binding of quarks inside hadrons.

Massless quarks have separately conserved left-handed and right-handed spin components. When the quarks have mass and the chiral symmetry is spontaneously broken, both components mix, giving rise to mass as well as mesons, such as π and σ, as composite quark-antiquark pairs.

In QCD, the quark condensate is believed to be a manifestation of spontaneous breaking of chiral symmetry. The quark condensate is a condensate of quark-antiquark pairs in a vacuum and its strength refers to the expectation value of the scalar density of quarks in a vacuum. When chiral symmetry is spontaneously broken, the quark condensate acquires a non-zero value, which leads to the generation of mass. In this sense, the quark condensate can be seen as a measure of the strength of chiral symmetry breaking. In particular, the behavior of the quark condensate is sensitive to the temperature and density of the system, and it can be used to study the behavior of matter under extreme conditions, such as inside quark-gluon plasma or neutron stars.

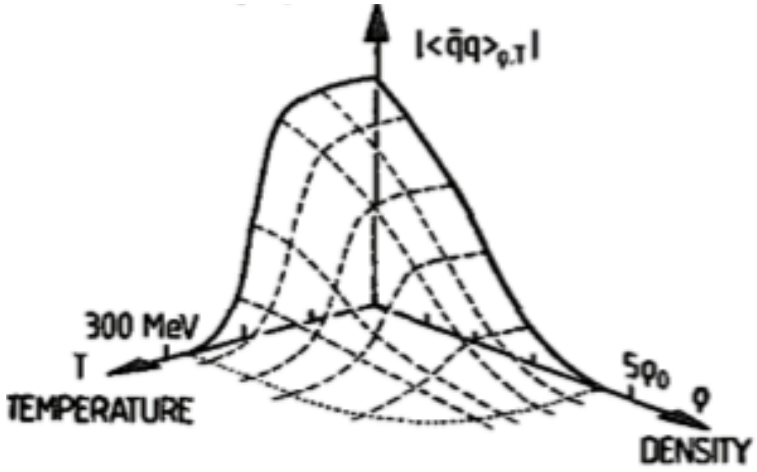

Figure 2: The condensate $<\bar{q}q>$ as a function of density ρ and temperature T. The density is given in units of nuclear matter density $\rho_0 = 0.17fm^{-3}$[2]

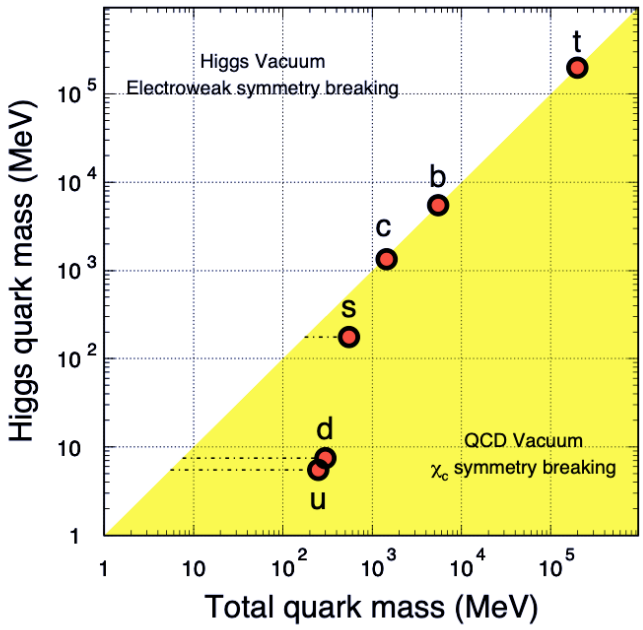

Figure 3: Quark masses in the QCD vacuum and the Higgs vacuum. A large fraction of the light quark masses is due to the chiral symmetry breaking in the QCD vacuum.[3]

2.5 Heavy ion collision

Heavy-ion collisions are experiments in which high-energy ions are used to acquire knowledge about the properties of elementary particles and nuclear physics. Heavy ion collision refers to the collision of two atomic nuclei with a high relative velocity, typically at extremely high energy levels in particle accelerators. These collisions are performed using particle accelerators, and the resulting high-energy interactions allow scientists to probe the behavior of subatomic particles, such as quarks and gluons, and study the properties of the quark-gluon plasma (QGP), a state of matter thought to have existed in the early universe.

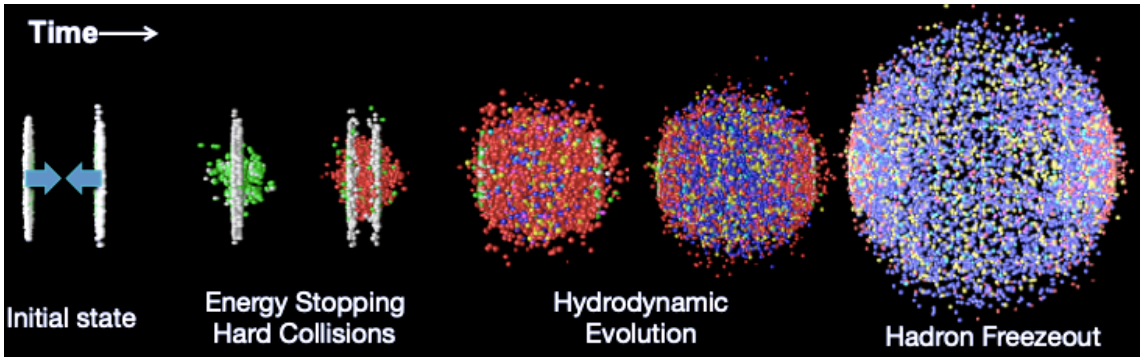

Figure 4: The time evolution of a high-energy heavy-ion collision[4]

2.5.1 Quark deconfinement

Quark deconfinement at extremely high temperatures refers to the transition of quarks from being confined within hadrons to existing as free, unbound particles. This transition occurs when the temperature of the system becomes so high that the strong force, which binds quarks within hadrons, is no longer able to keep them confined.

At high temperatures, the energy of the particles in a system can become so great that the strong force holding the quarks inside hadrons is no longer sufficient to overcome the thermal motion of the particles. As a result, the quarks can break free from the hadrons and exist as individual entities. This state is referred to as a quark-gluon plasma (QGP).

The study of quark deconfinement at extremely high temperatures is important for understanding the behavior of matter under extreme conditions and for exploring the conditions that existed in the early universe a few microseconds after the Big Bang because the QGP is believed to have existed in the early universe a few microseconds after the Big Bang. Experiments at high-energy particle colliders, such as the Relativistic Heavy Ion Collider (RHIC), have provided evidence for the existence of the QGP. Currently, experimental facilities such as the Relativistic Heavy Ion Collider (RHIC) at Brookhaven National Laboratory and the Large Hadron Collider (LHC) at CERN are the only laboratories capable of generating QGP.

2.5.2 Partial restoration of chiral symmetry

At high temperatures or densities, the conditions can change in a way that chiral symmetry is partially or completely restored. This can lead to changes in the properties of light vector mesons, such as a reduction in their masses, which provides information about the extent of chiral symmetry breaking and the behavior of the strong force in these extreme environments. The restoration of chiral symmetry at high temperatures has been predicted by quantum chromodynamics (QCD), the theory of the strong interaction between quarks and gluons. It has been studied in numerical simulations and in experiments at particle accelerators, such as the Relativistic Heavy Ion Collider (RHIC) at Brookhaven National Laboratory and the Large Hadron Collider (LHC) at CERN. Light vector mesons, such as the ρ and ω mesons, are considered to be sensitive probes of chiral symmetry breaking in QCD. This is because the properties of light vector mesons, such as their masses and decay widths, can be influenced by their mixing with other mesons that are related by chiral symmetry, such as the pion. The study of chiral symmetry restoration is of great interest because it provides insight into the behavior of hot and dense matter, which is thought to have existed in the early universe shortly after the Big Bang. It is also relevant to the study of neutron stars, where matter is thought to be in a similar state.

2.6 Results of experiments to discover chiral symmetry restoration at high-temperature

The exact mechanism by which the mass of vector mesons changes in the QGP is not well understood, and is the subject of ongoing research and analysis. However, it is thought to be related to the interactions between the vector mesons and the QGP created by the heavy-ion collisions.

High-energy heavy-ion collisions have measured the mass distribution of light vector mesons by lepton pair measurements. The NA45 measurements of e^+e^- and the NA60 measurements of $\mu^+\mu^-$ measurements have been performed at the CERN SPS accelerator. The NA60 experiment reports results that support the broadening of ρ meson[22]. And the PHENIX measurement of e^+e^- has been performed at the RHIC[23]. The measurement is important because the mass modifications of light vector mesons at LHC energies has not been found yet.

Aspects from computer science, Wilson's lattice gauge theory and recent advances in the use of computers have made it possible to investigate both the confinement problem and chiral symmetry breaking in a fairly quantitative way. Both phenomena are shown to actually occur in QCD and, moreover, to undergo two types of phase transitions at finite temperatures. One is the breaking of confinement and the other is the restoration of chiral symmetry.

2.7 Purpose of this study

The purpose of this study is to evaluate the detectability and establish the method for evaluation of mass modification with pole mass broadening, and dropping-and-broadening scenarios. This is toward the invariant mass analysis in Pb-Pb in Run 3 at ALICE, and discovering the mass modification due to chiral symmetry restoration.

3 Experimental Setup

3.1 Large Hadron Collider

The Large Hadron Collider, LHC[10][11][12], is the world's largest particle accelerator. It was built in The European Organization for Nuclear Research, CERN in Geneva, Switzerland, and has been in operation since 2008. The LHC is installed in the about 27 km circumference tunnel where the Large Electron-Positron Collider, LEP located, as its successor. It is in the depth of 50 to 175m underground. The accelerator consists of an acceleration cavity to accelerate charged particles to close to the speed of light and a superconducting magnet to maintain the trajectory of the accelerated particles. Charged particles are accelerated in opposite directions in two rings and collide at the collision point. The collisions produce high-energy showers of particles, which can then be detected and analyzed by detectors surrounding the collision point. The detectors collect data on the properties and interactions of the particles to study the fundamental structure of matter and the forces that govern it. The main objectives include the discovery of the Higgs boson, and the verification of supersymmetry theory which is a beyond Standard Model. There is also the expectation of discovering entirely new phenomena never considered before in high-energy regions. In 2012, ATLAS and CMS, which are the major experiments at the LHC, discovered the Higgs boson[8][9]. Supersymmetry hasn't be found as yet. In addition to this, in 2015, the LHC discovered a new particle, the pentaquark, which is composed of five quarks instead of the usual two or three. The LHC has also been used to search for dark matter and dark energy, two mysterious substances that make up a significant portion of the universe. Although dark matter and dark energy have never been directly detected, they are believed to play a crucial role in the formation and evolution of galaxies. By colliding particles at high energies, the LHC may be able to produce dark matter particles. The LHC as the energy frontier is also essential to research for the mysteries of the universe immediately after the Big Bang and the beginning of the universe, and it aims to produce results that will deepen our understanding of more fundamental aspects in ultramicroscopic world.

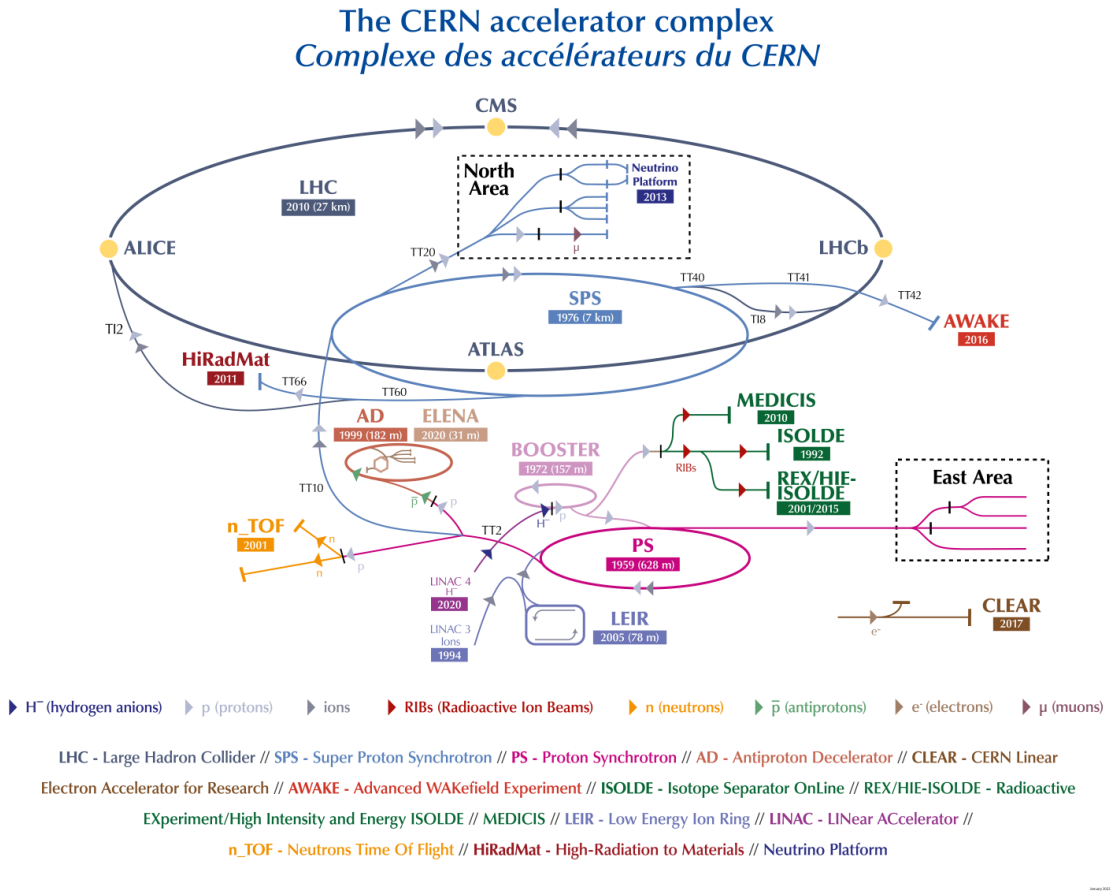

Figure 5: CERN's accelerator complex[5]

3.2 ALICE detector

Experimental facilities have been installed at several collision points on the LHC and ALICE detector is one of them. Among the experiments at the LHC, A Large Ion Collider Experiment, ALICE is the only experiment that focuses on understanding the properties of quark-gluon plasma, QGP produced by lead nucleus collisions. The QGP state can be determined by precisely measuring the produced particles by collisions. Therefore, to achieve this objective, the ALICE detector is designed to measure a wide energy/momentum range so that it can measure a variety of produced particles. One of the key goals of ALICE is to study the quark-gluon plasma (QGP). And two major themes of ALICE experiment are the elucidation of quark-confinement and the elucidation of mass acquisition mechanism.

The ALICE detector consists of several main components, including the central tracking system, the central barrel, the muon spectrometer, and the electromagnetic calorimeter. The central tracking system, located at the center of the ALICE apparatus, consists of a silicon pixel tracker, a silicon strip tracker, and a time projection chamber, which measure the trajectories of particles produced in the collisions. The central barrel, located around the central tracking system, contains the time-of-flight detector and the transition radiation detector, which measure the velocity of charged particles and provide particle identification.

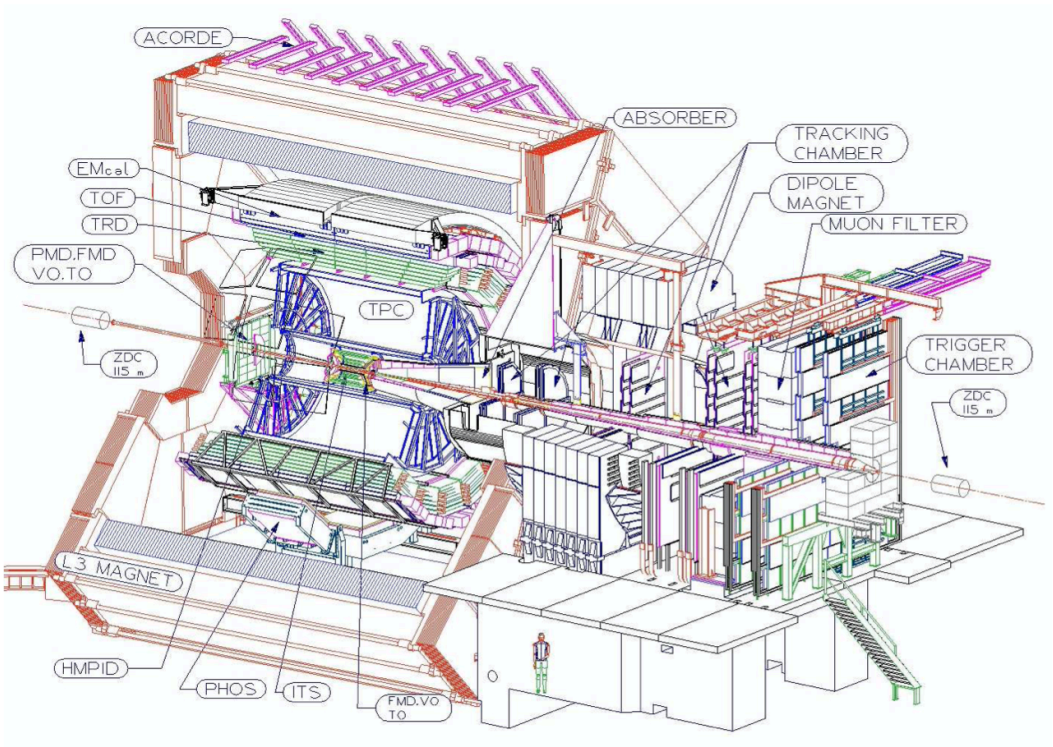

Figure 6: General view of the ALICE detector[6]

In Run3, the ALICE experiment introduce a new detector, the Muon Forward Tracker, MFT[24][25]. Until Run 2, the only forward muon detector was a muon spectrometer, but this system used a front absorber to select muons, which eliminated many hadrons, but also caused multiple Coulomb scattering with the absorber. The muon trajectory is measured after the multiple Coulomb scattering, but the trajectory near the collision point before the scattering is not clear. If the track near the collision point is unclear, the decay angle of the light vector meson when it decays into a muon pair becomes ambiguous, which adversely affects the mass resolution when an invariant mass is reconstructed from the muon pair. The MFT detector is installed in front of the absorber, thus avoiding this problem.This allows run3 to measure muons more accurately.

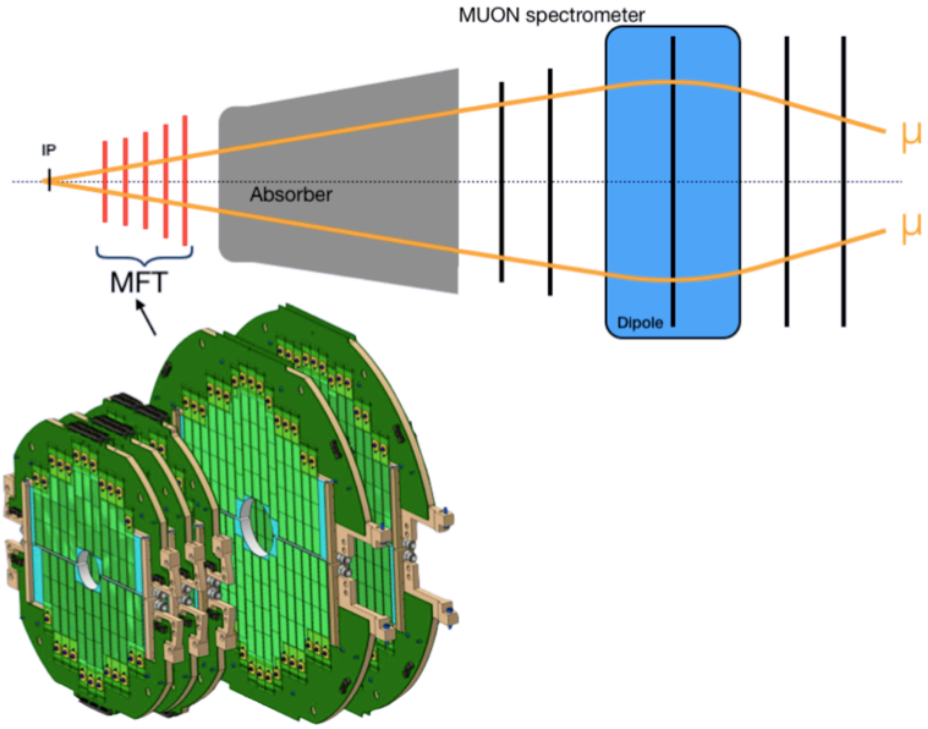

Figure 7: The MFT image[7]

4 Simulation and Result

In this section, detectability for ω mass modification is evaluated. The data samples of pp collisions are used, despite this study is toward mass distribution analysis in Pb-Pb collisions in Run 3. This is for two reasons. The first reason is the large amount of background events in Pb-Pb collisions. Clearer evaluation can be realized by using pp data. The second reason is related to triggers. In Pb-Pb collisions in Run 2, a trigger threshold of $p_T = 1$GeV/c was applied. Due to this, $p_T < 2$ GeV/c region couldn't be measured. For these reasons, data samples of pp collisions in Run 2 is used for this study. In Run 3, there will be no p_T trigger thresholds.

In this study, three mass modification scenarios are considered. They are dropping pole scenario, broadening pole scenario and pole dropping and broadening scenario respectively. In the previous study[26], detectability of ω meson mass modification with dropping pole scenario was studied. The method for study is based on this previous study. It is applied and extended to other scenarios.

The procedures for detectability evaluation consists of 3 steps. For the first step, the dimuon invariant mass spectrum created from the collected data is analyzed into components. In the second step, this analyzed components is used to create pseudo-spectra of dimuon invariant mass reflected the ω meson mass modification scenario using a Monte Carlo simulation. Inthe final step, the pseudo-spectra are fitted with a function that does not assume mass modification and a function that does, respectively, and the difference of χ^2 values of fittings is used to evaluate the detectability. The smaller the difference of χ^2 values, the lower the detectability, and the larger the χ^2 value of non-modification assumed function than that of modification assumed function, the higher the detectability.

4.1 Analysis of invariant mass distribution

4.1.1 Data set

In this study, the used data is samples of pp collisions at $\sqrt{s} = 13$ TeV with ALICE detector in 2016. Run periods are LHC16f, LHC16g, LHC16h, LHC16i, LHC16j, LHC16k, LHC16l, LHC16m, LHC 16n, and LHC16o.

4.1.2 Invariant mass reconstruction

When focusing on a system, "a mass" as when the system is a particle can be considered. It is called invariant mass. Invariant mass M is described like

$$M = \sqrt{(\mathbf{p_1} + \mathbf{p_2} + ... + \mathbf{p_n})}, \tag{1}$$

where

$\mathbf{p_1}, \mathbf{p_2}, ..., \mathbf{p_n}$: four-momentum of each patricle in the system

Invariant mass is Lorentz invariant. A mass of a parent particle can be reconstructed by using invariant mass. Invariant mass of a parent particle can be reconstructed from mass m, energy E and momentum p of its daughter particle by using the law of conservation of energy and the law of conservation of momentum. The reconstructed invariant mass is treated as histogram using ROOT. In this analysis, the bin width of histograms is 10 MeV/c^2 per each. Since $\omega \to \mu\mu$ decay process is focused on, this spectrum analysis begins with the invariant mass spectrum reconstructed from dimuon of opposite charges decayed in same event. However, it is not possible to know which dimuon is actually the one which ω meson has decayed. Some components of the spectrum are from uncorrelated muon pairs. This is called combinatorial background. Combinatorial background can be estimated by reproducing a invariant mass distribution which is constructed from uncorrelated muon pairs. Consequently, the component from correlated muon pairs can be extracted. A technique for reproducing a distribution of uncorrelated muon pairs is like-sign pair technique[27].

4.1.3 Subtraction of uncorrelated background

The like-sign pair technique is a method used in particle physics to estimate the number of uncorrelated particle-antiparticle pairs in a sample of data. In the like-sign pair technique, the sample of particle interactions is first divided into two groups based on the electric charge of the particles. One group contains particles with a positive electric charge, and the other group contains particles with a negative electric charge. The number of like-sign particle-antiparticle pairs, i.e., pairs with the same electric charge, is then counted for each group.
Since the number of uncorrelated particle-antiparticle pairs should be equal in the two groups, the average number of like-sign pairs can be used as an estimate of the number of uncorrelated pairs. This estimate can then be subtracted from the total number of opposite-sign pairs to obtain an estimate of the number of correlated pairs. This is given by:

$$N_{Corr.} = (N_{\mu^+\mu^-})_{same} - N_{Comb.} \,. \tag{2}$$

$N_{Corr.}$: Number of correlated muon pairs
$N_{Comb.}$: Number of combinatorial background
$(N_{\mu^+\mu^-})_{same}$: Number of opposite charged muon pairs between same event

Here, the combinatorial background is estimated by:

$$N_{Comb.} = 2C_{Asym.}\sqrt{(N_{\mu^+\mu^+})_{same}(N_{\mu^-\mu^-})_{same}} \,. \tag{3}$$

$(N_{\mu^+\mu^+})_{same}$: Number of positive charged muon pairs between same event
$(N_{\mu^-\mu^-})_{same}$: Number of negative charged muon pairs between same event

The factor $C_{Asym.}$ is a correction factor for an asymmetry between positive and negative charges. It accounts for a production asymmetry between positively charged particles and negatively charged particles, or a detector trigger/acceptance bias relative to the particle charge. This factor is obtained from not only muon pairs between the same event, but also muon pairs between different events. The $C_Asym.$ factor is calculated by:

$$C_{Asym.} = \frac{(N_{\mu^+\mu^-})_{mixed}}{2\sqrt{(N_{\mu^+\mu^+})_{mixed}(N_{\mu^-\mu^-})_{mixed}}} \,. \tag{4}$$

$(N_{\mu^+\mu^-})_{mixed}$: Number of opposite charged muon pairs between mixed event
$(N_{\mu^+\mu^+})_{mixed}$: Number of positive charged muon pairs between mixed event
$(N_{\mu^-\mu^-})_{mixed}$: Number of negative charged muon pairs between mixed event

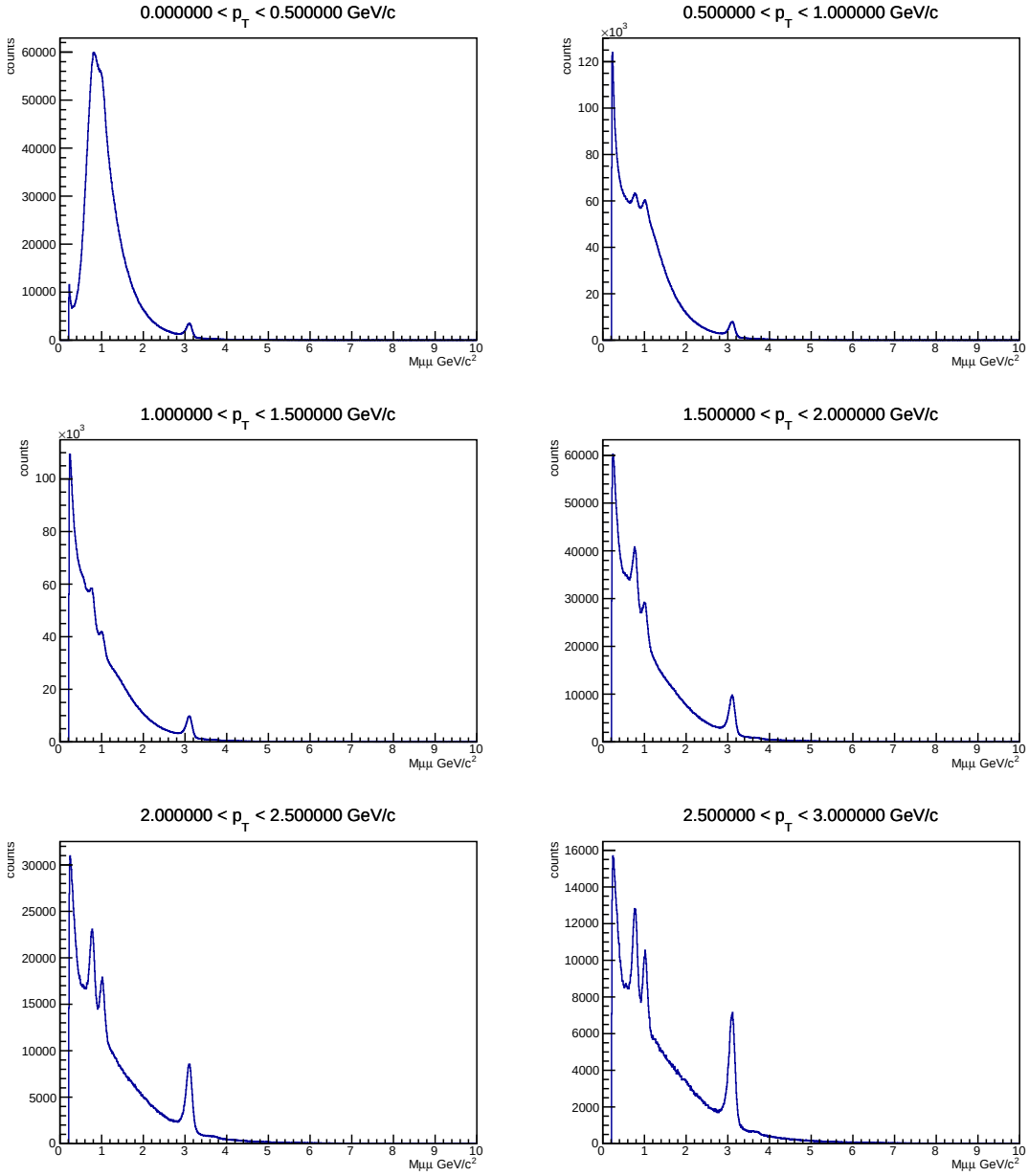

Figure 8: Dimuon invariant mass with opposite charged muon combinations in same event

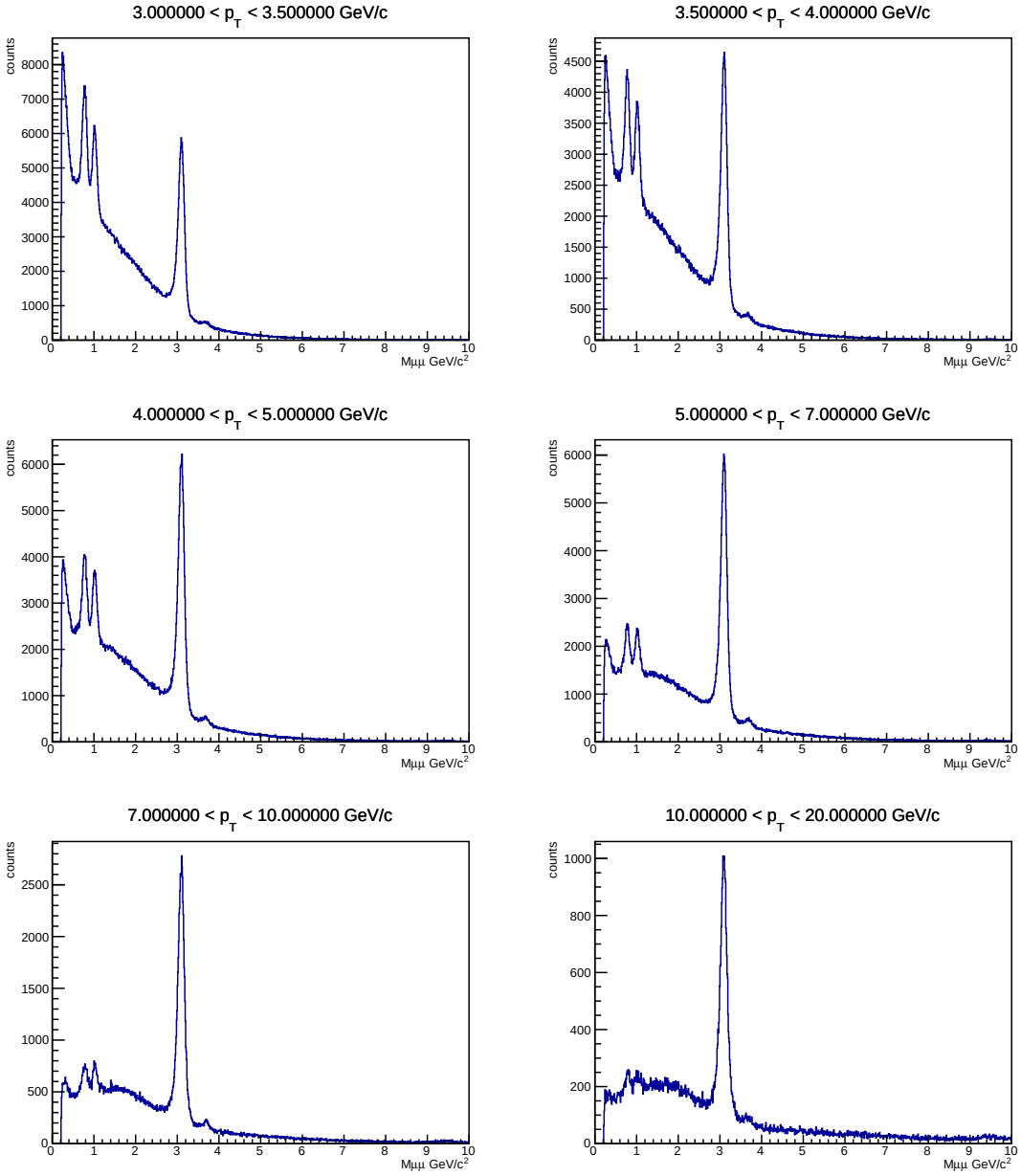

Figure 9: Dimuon invariant mass with opposite charged muon combinations in same event

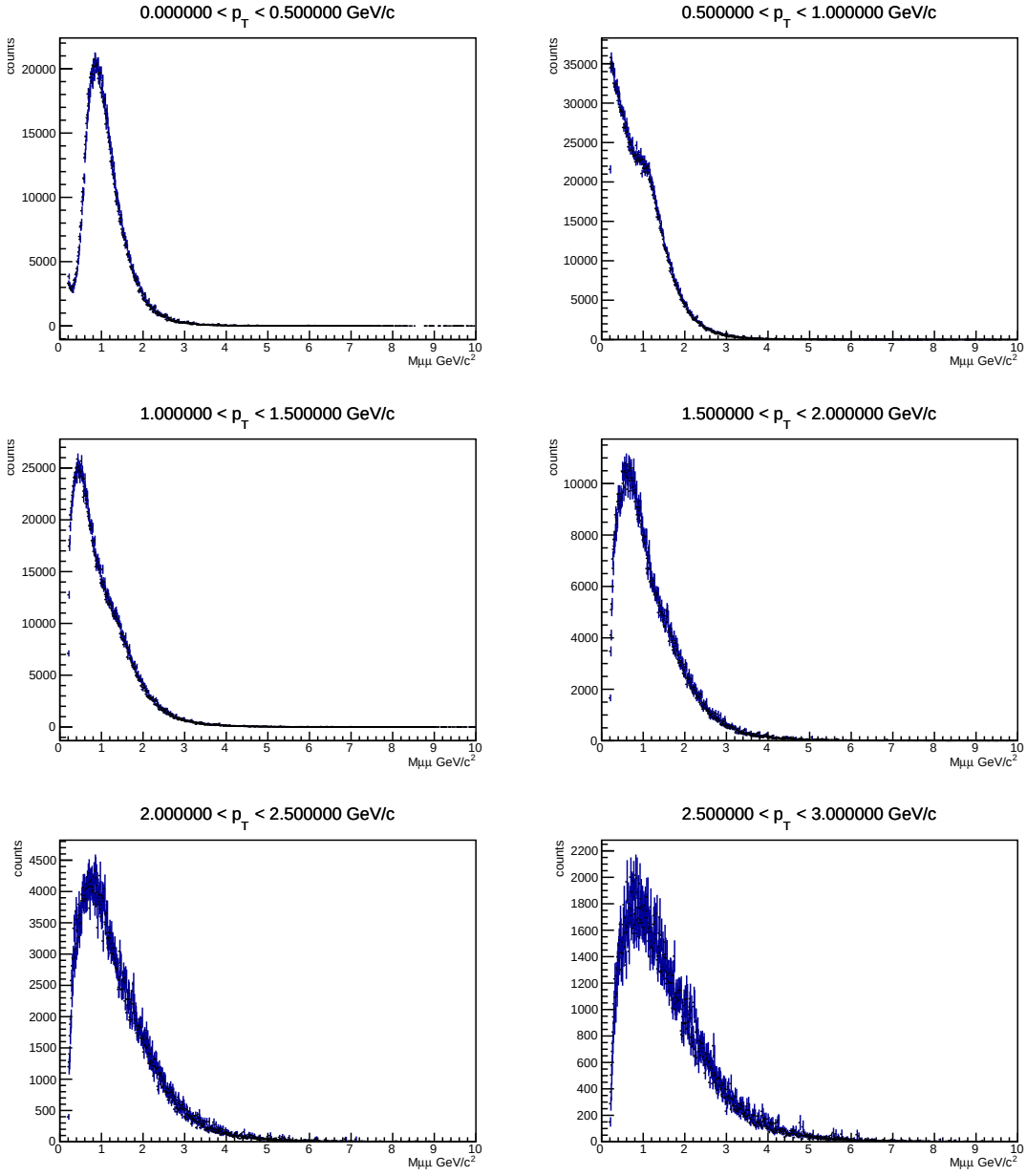

Figure 10: Dimuon invariant mass with positive charged muon combinations in same event

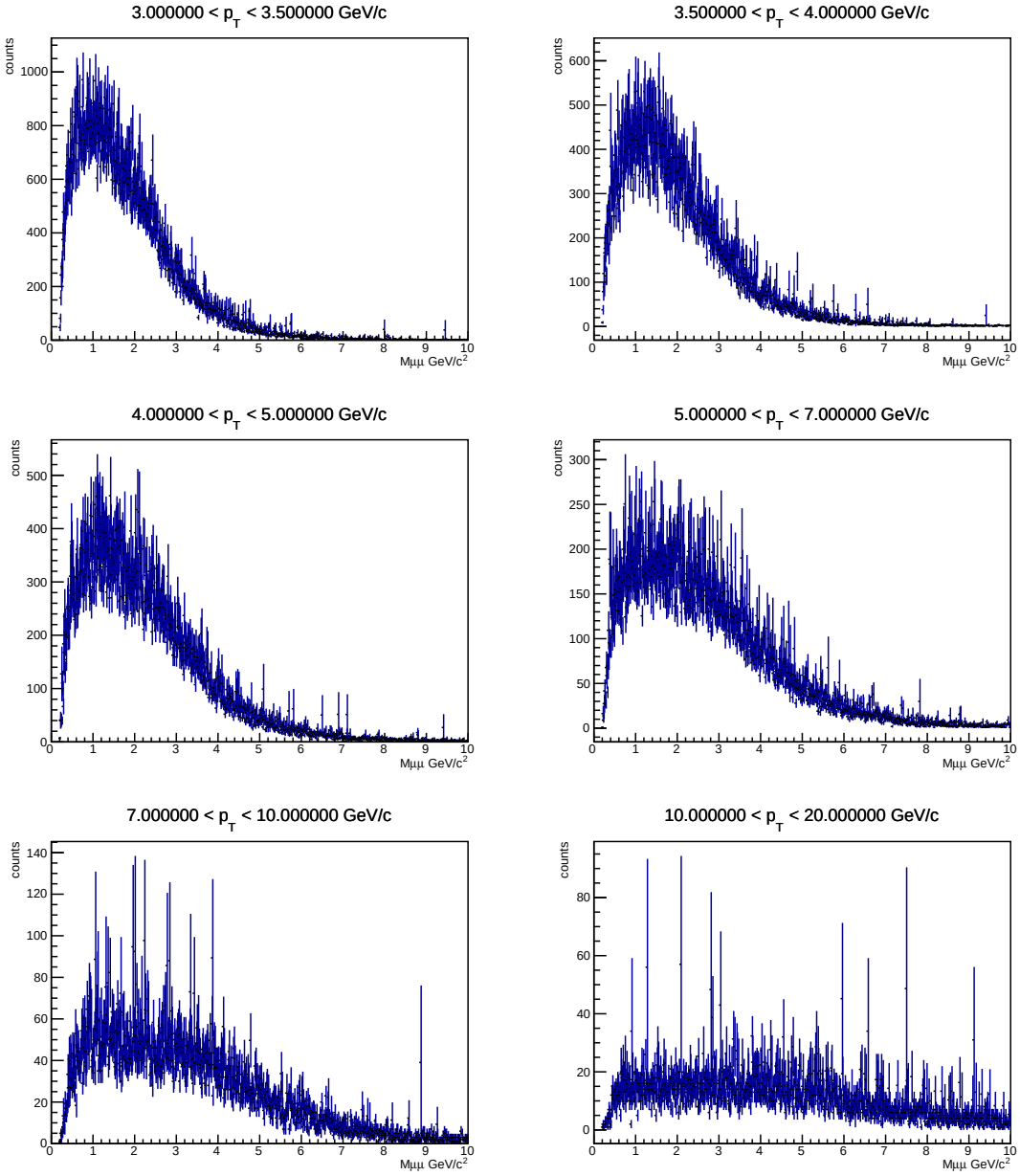

Figure 11: Dimuon invariant mass with positive charged muon combinations in same event

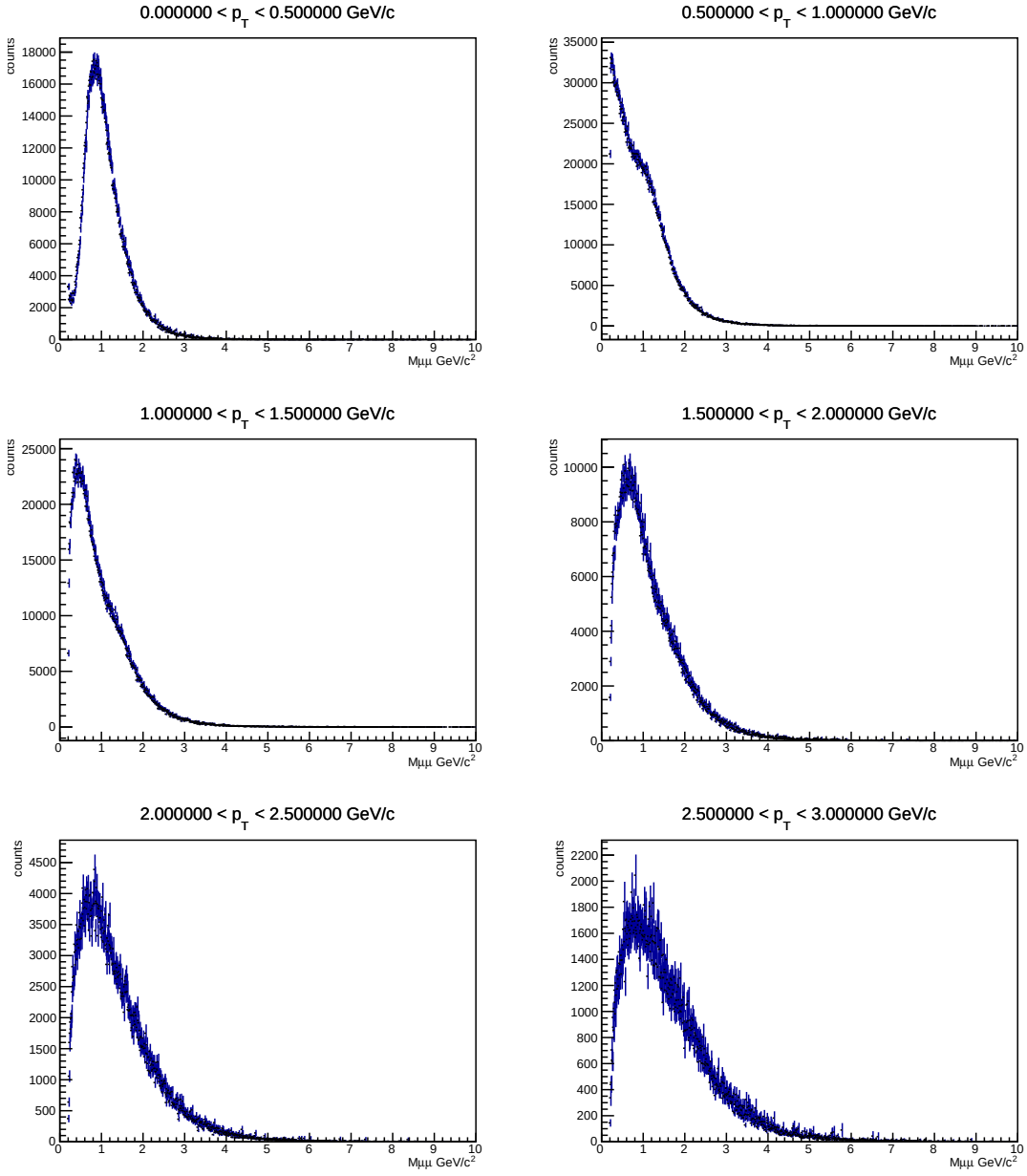

Figure 12: Dimuon invariant mass with negative charged muon combinations in same event

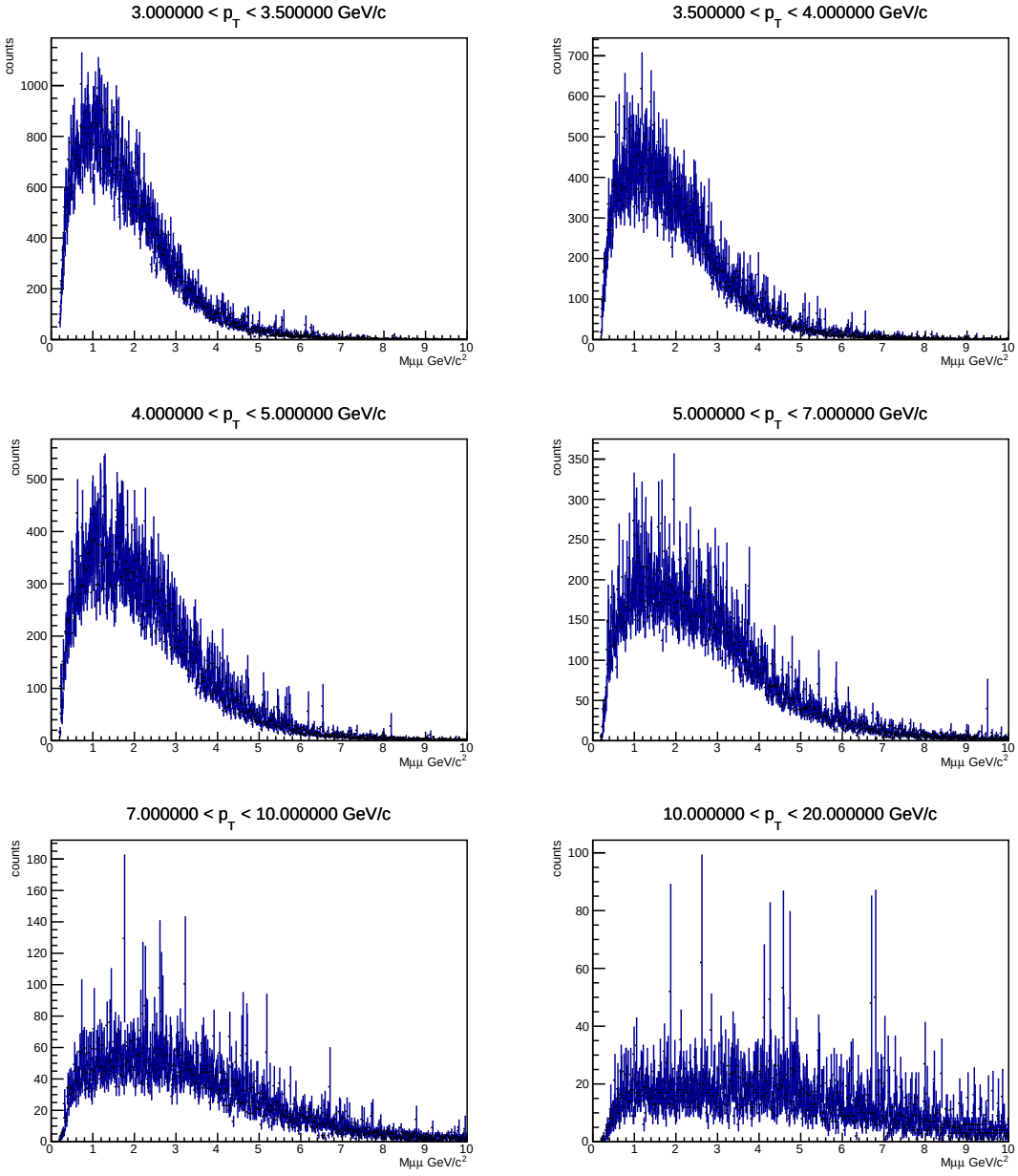

Figure 13: Dimuon invariant mass with negative charged muon combinations in same event

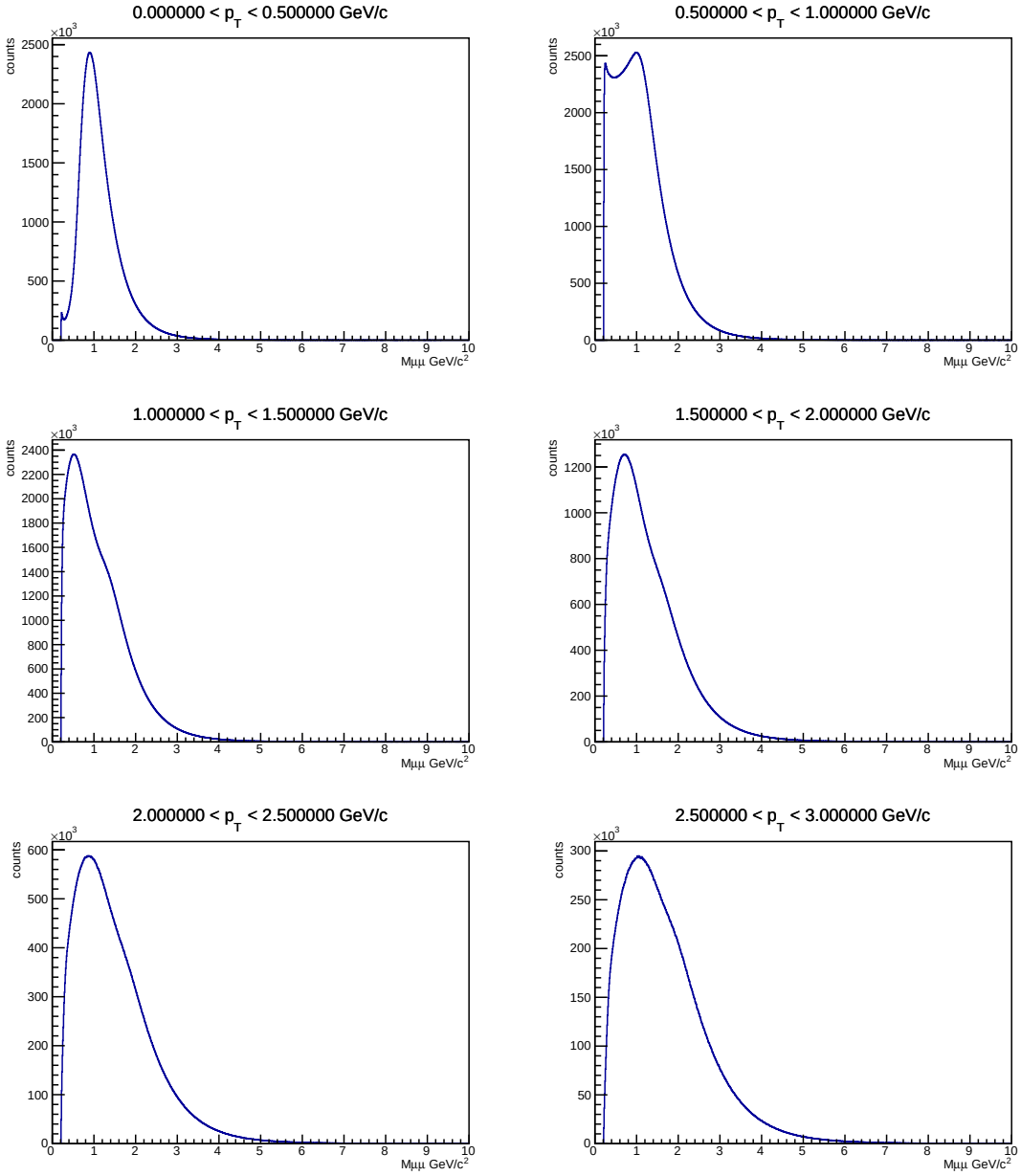

Figure 14: Dimuon invariant mass with opposite charged muon combinations between different events

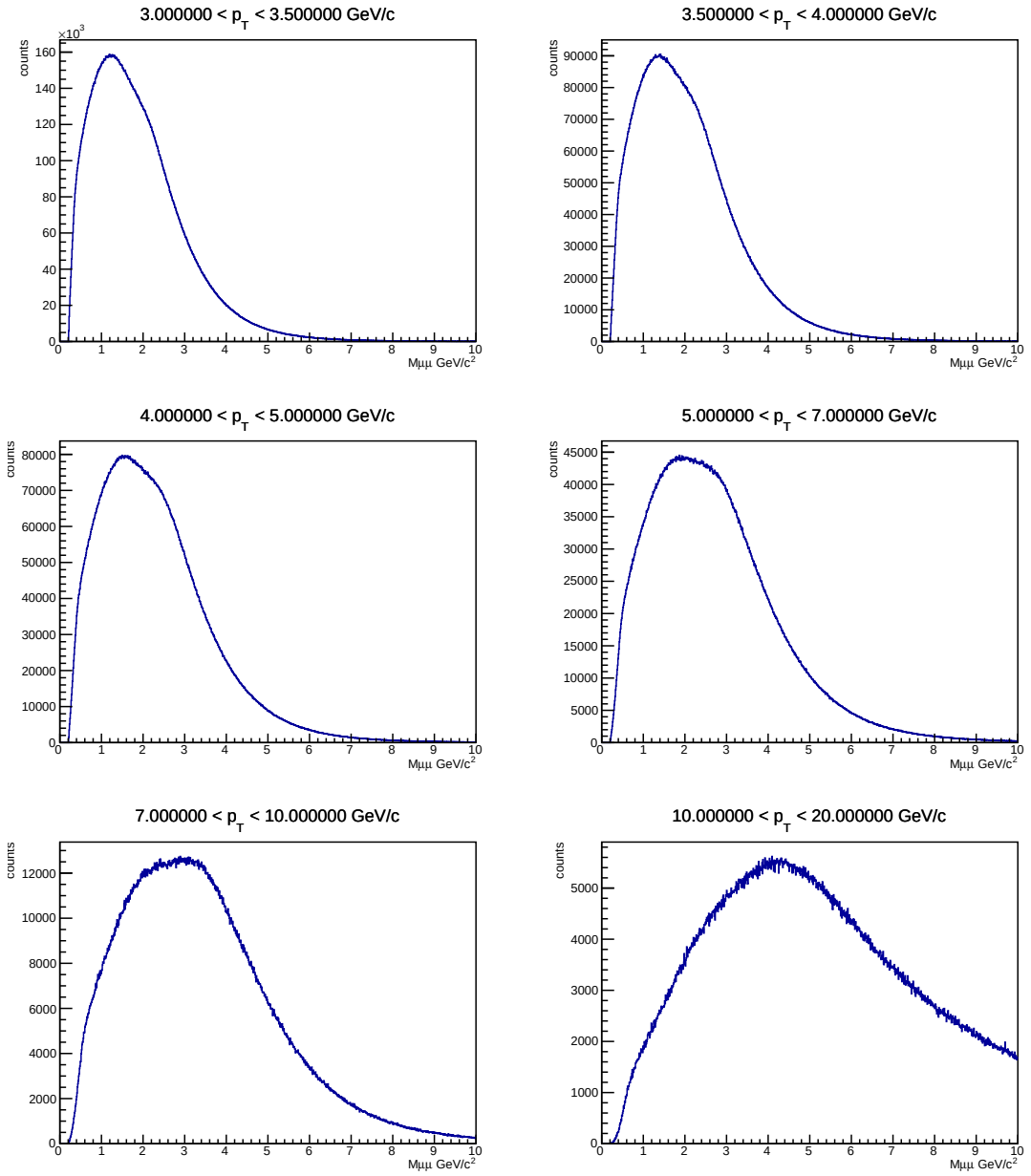

Figure 15: Dimuon invariant mass with opposite charged muon combinations between different events

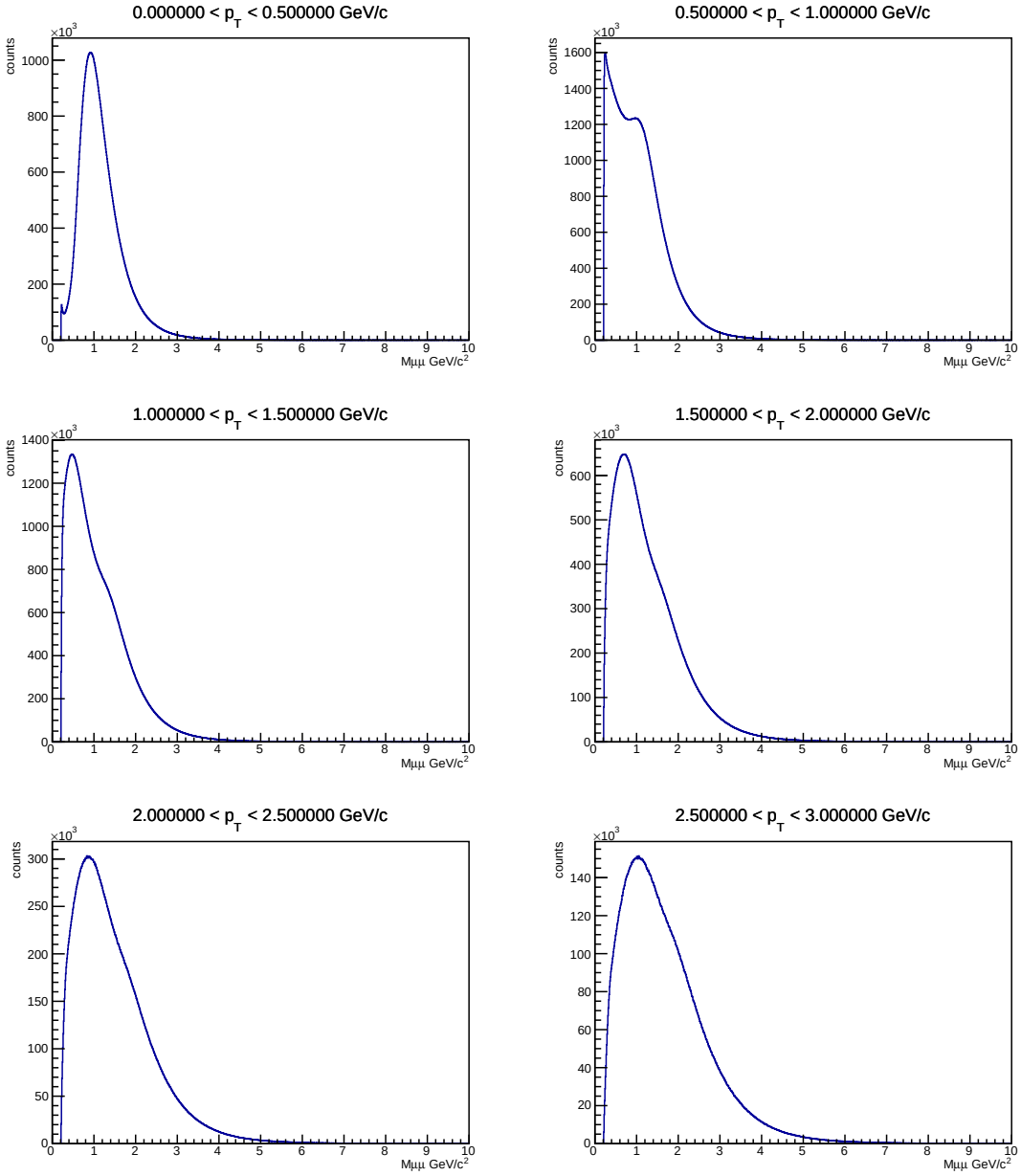

Figure 16: Dimuon invariant mass with positive charged muon combinations between different events

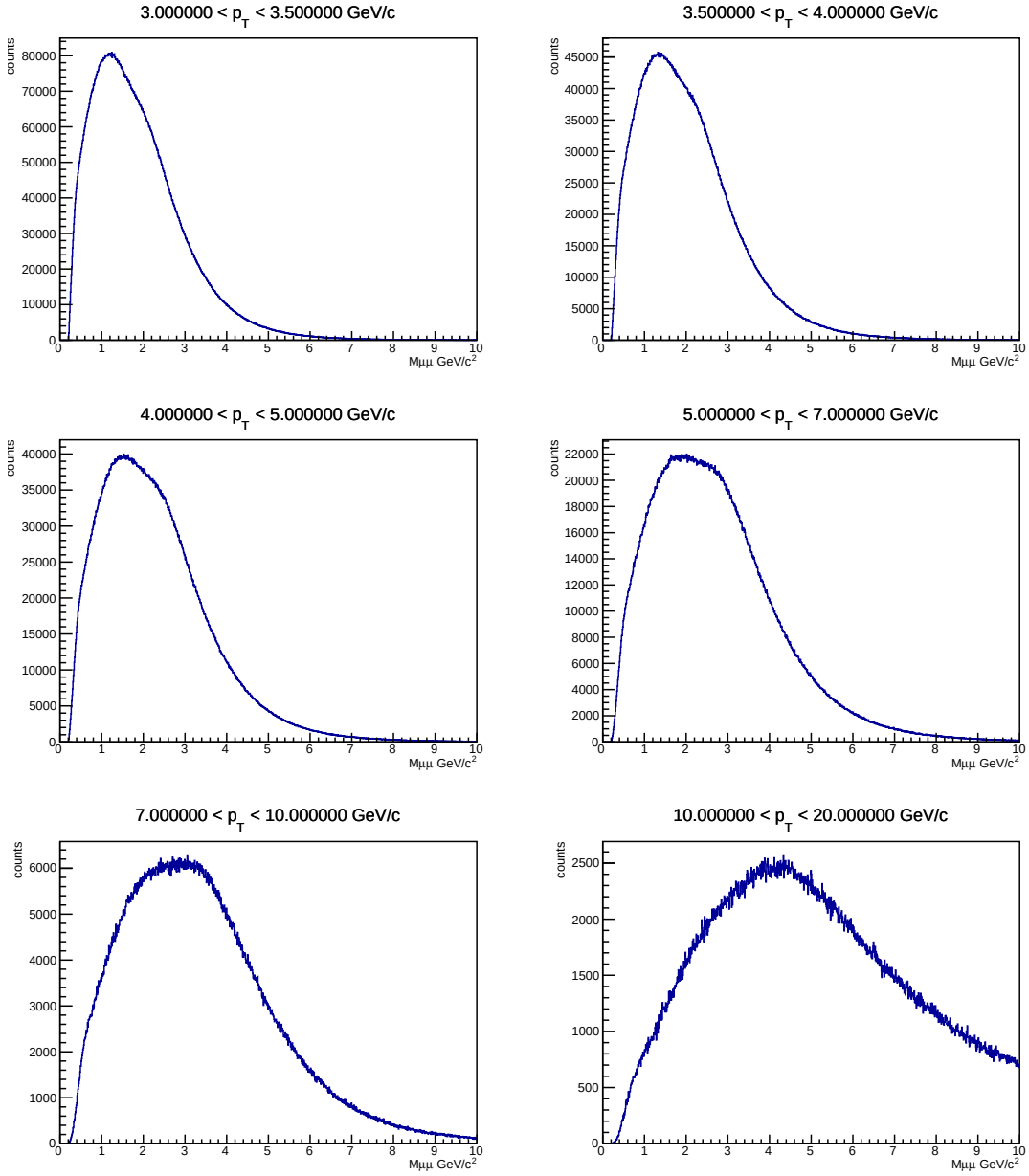

Figure 17: Dimuon invariant mass with positive charged muon combinations between different events

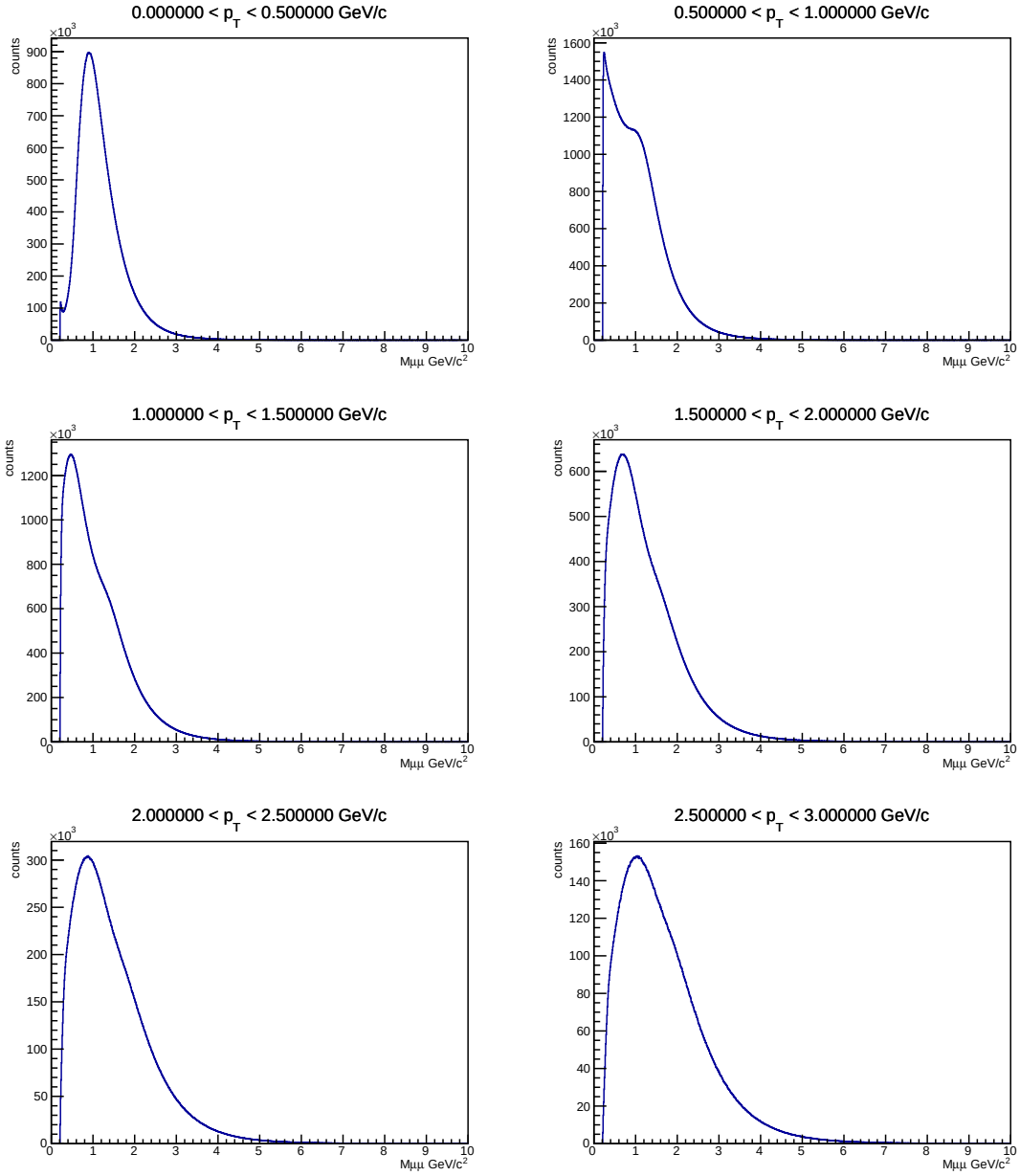

Figure 18: Dimuon invariant mass with negative charged muon combinations between different events

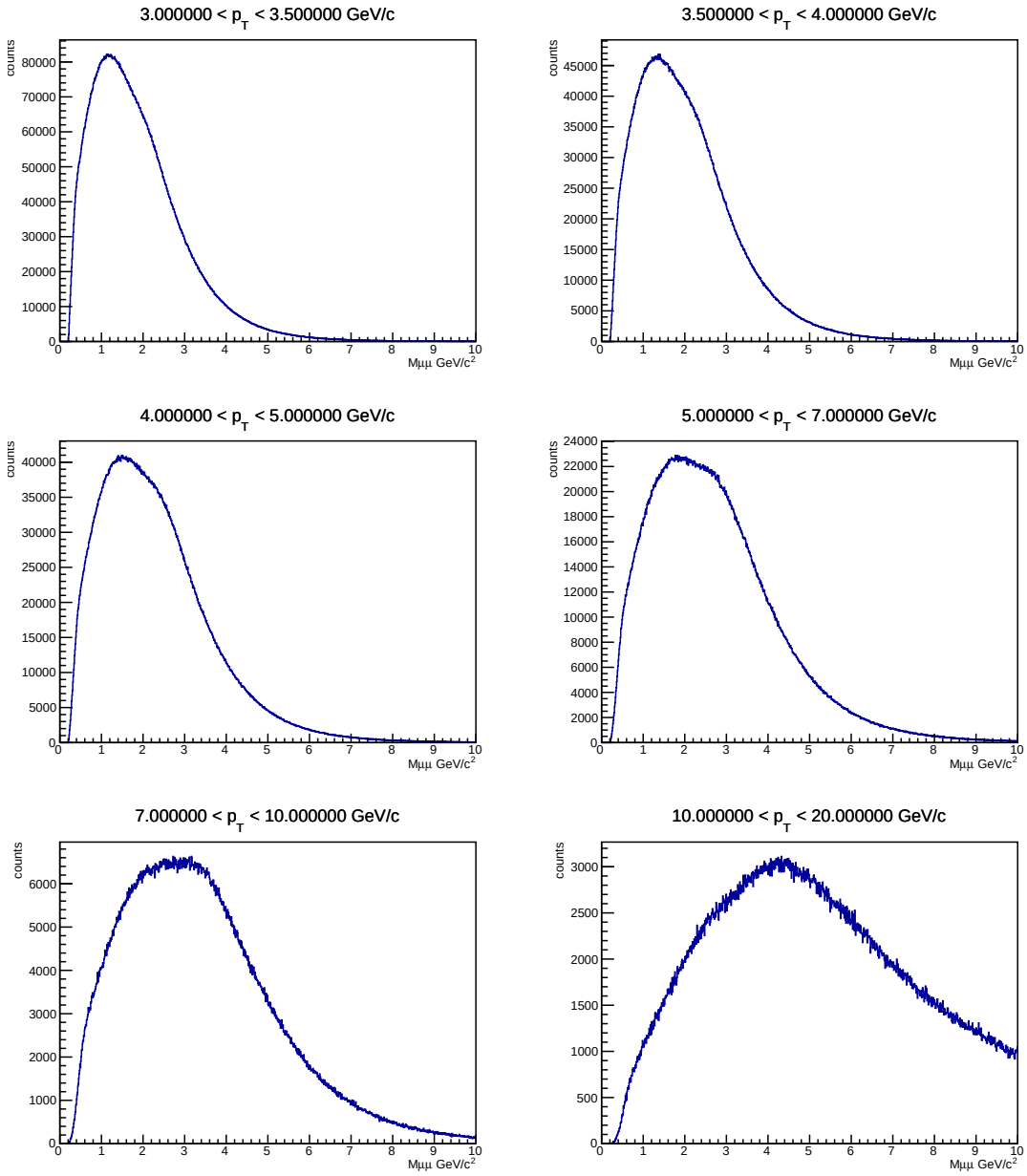

Figure 19: Dimuon invariant mass with negative charged muon combinations between different events

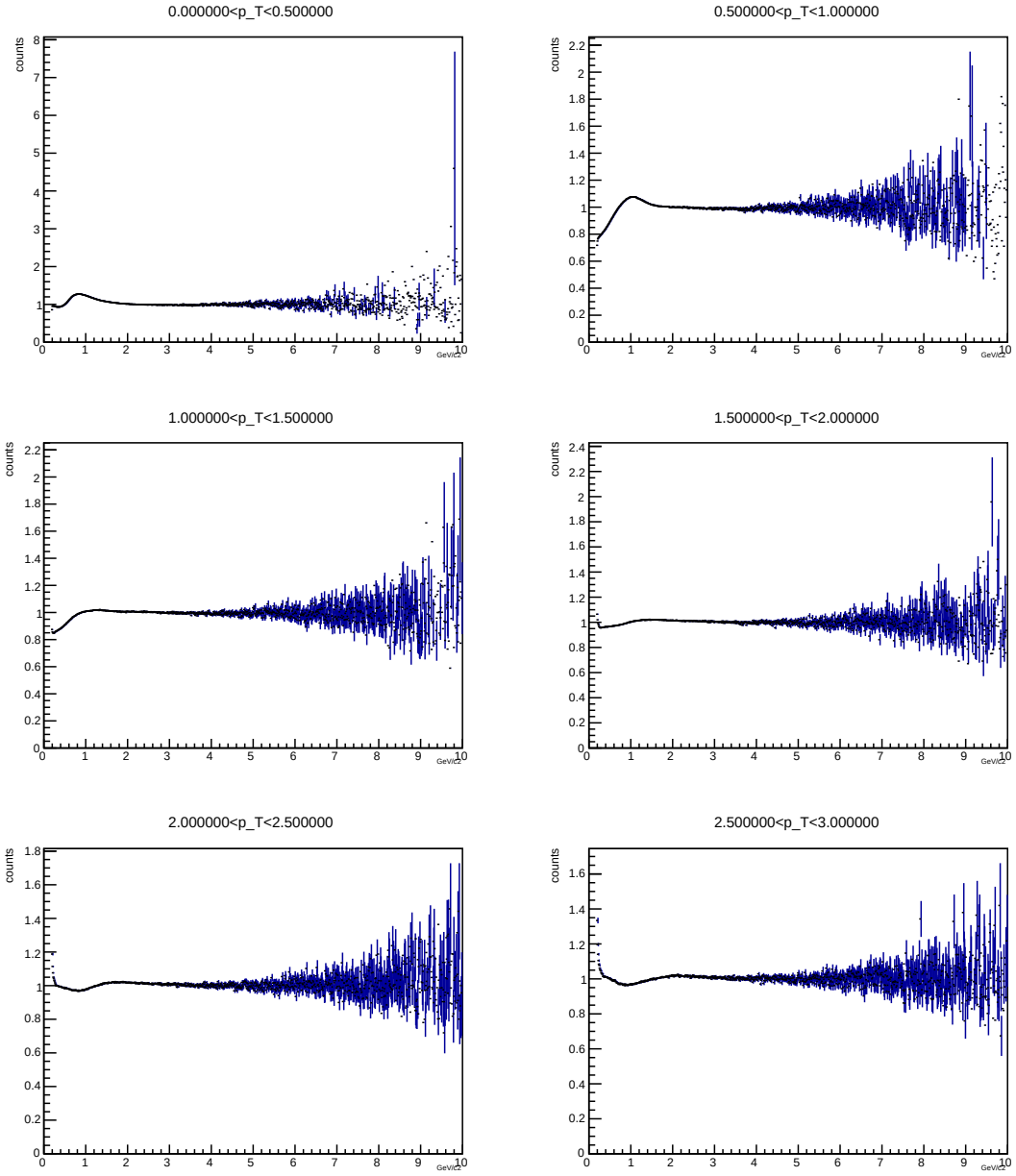

Figure 20: Rfactor1

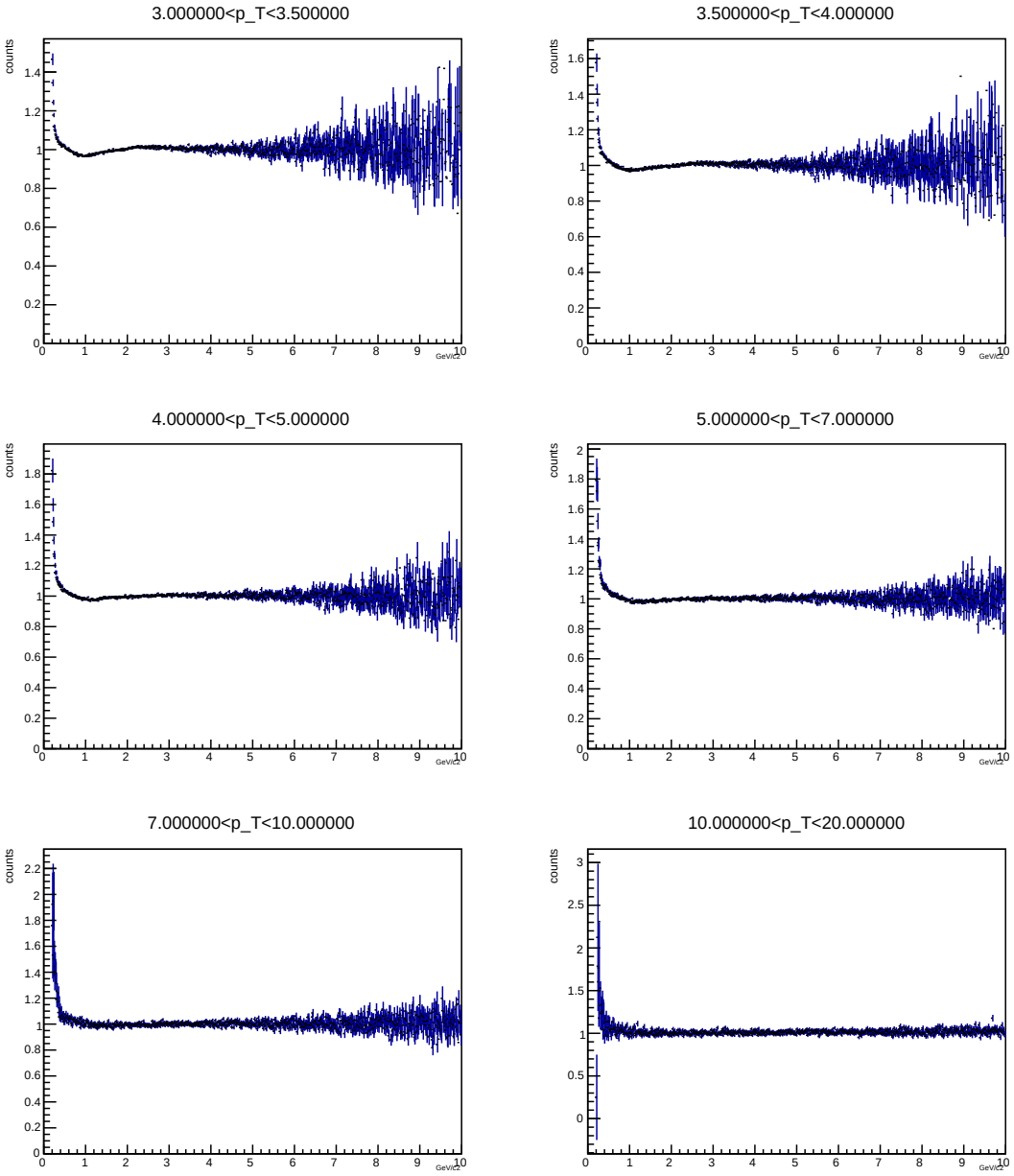

Figure 21: Rfactor2

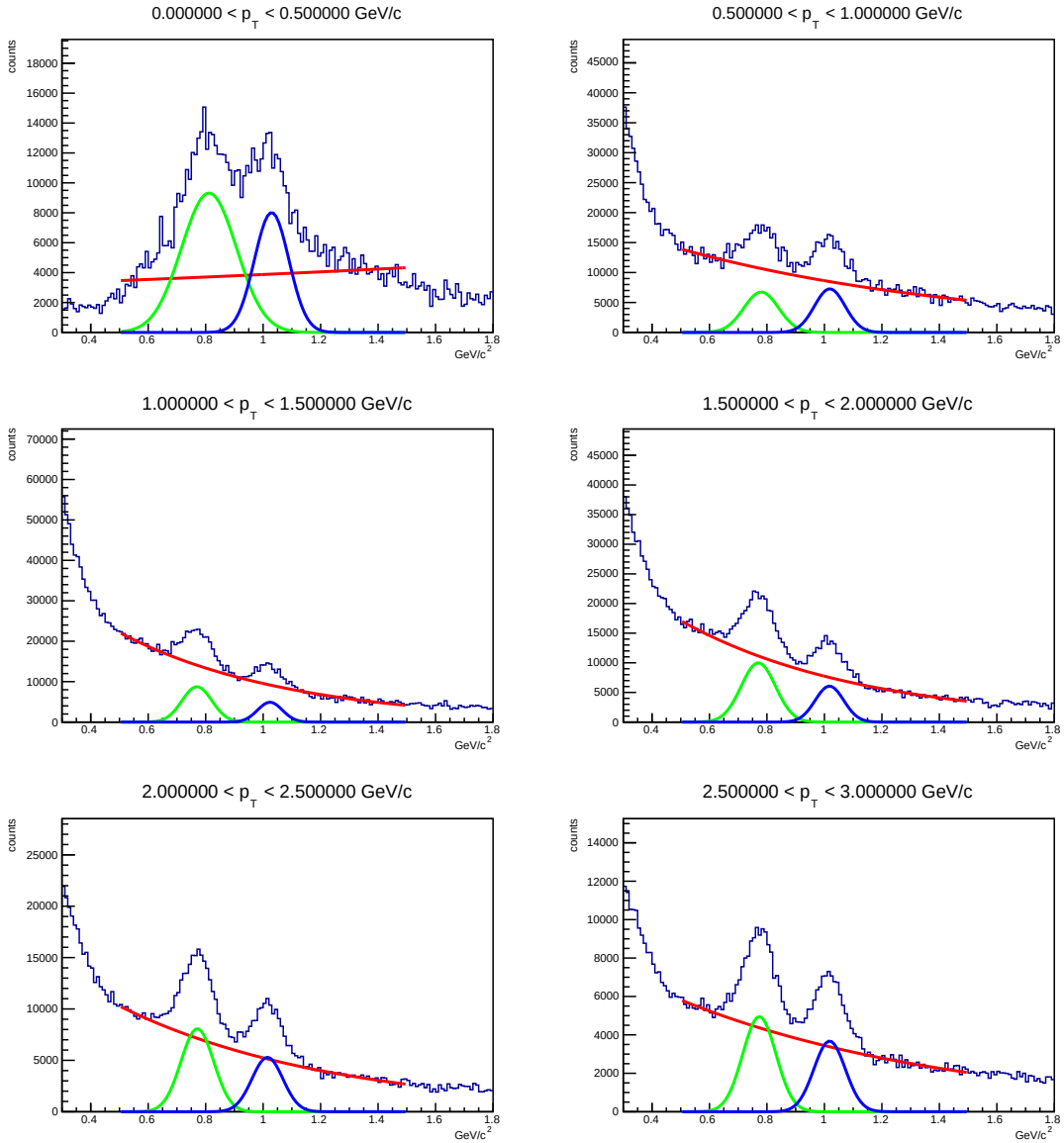

Figure 22: Correlated spectrum fitted by background and ω meson and ϕ meson in 0.5-1.5 GeV/c^2 region.

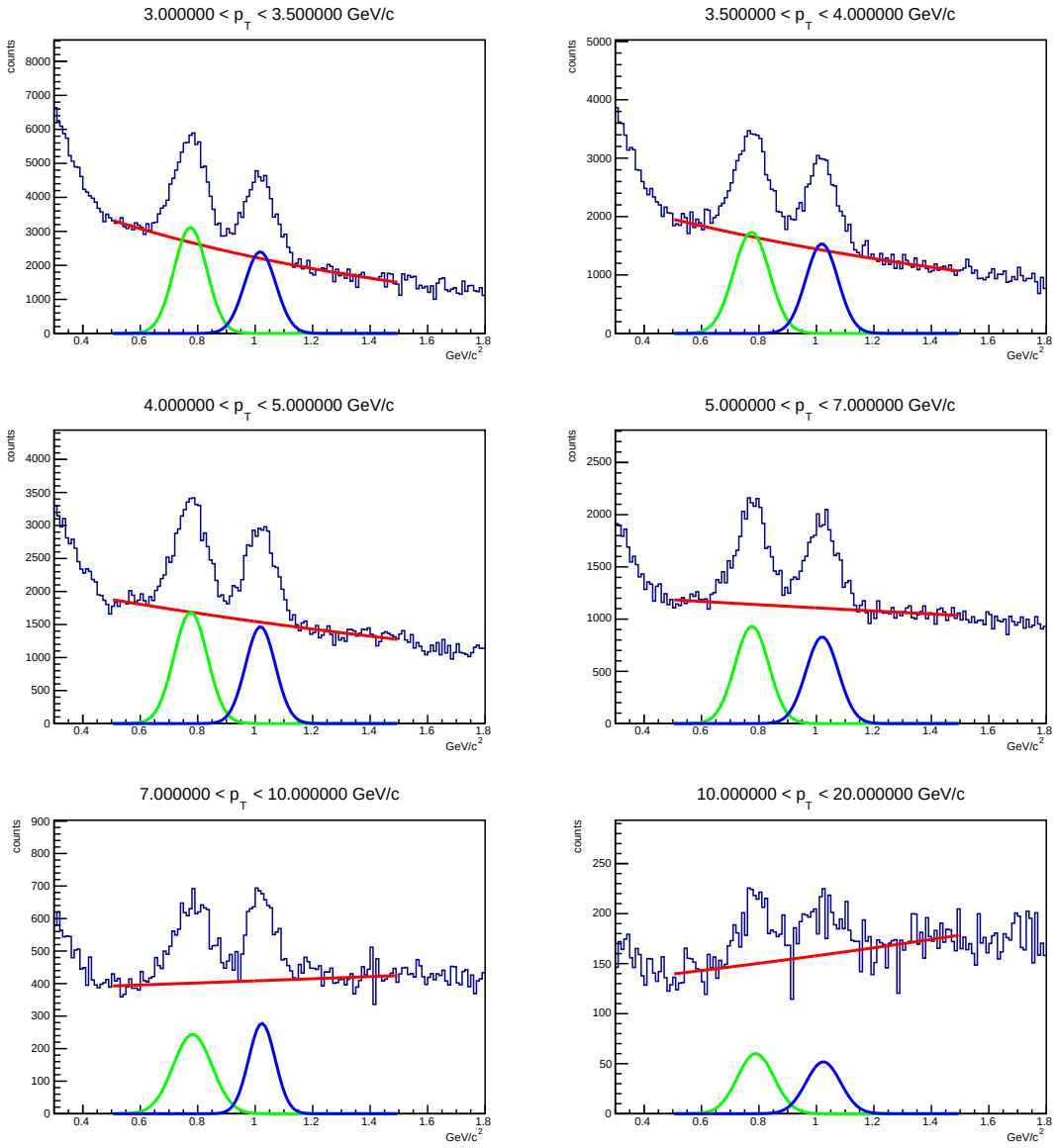

Figure 23: Correlated spectrum fitted by background and ω meson and ϕ meson in 0.5-1.5 GeV/c^2 region.

4.1.4 Fitting to correlated invariant mass distribution

In the last section4.1.3, invariant mass distribution only from correlated muon pairs has been obtained by extracting components from uncorrelated muon pairs with using like-sign pair technique. The ω meson, which is the modified target in this study, has the following mass properties in PDG: the Mass $m = 782.66 \pm 0.13$ MeV, the full width $\Gamma = 8.68 \pm 0.13$ MeV. Looking around this mass region, the ϕ meson peak which is from $\phi \to \mu\mu$ decays is a obvious composition. Its mass properties in PDG are: the Mass $m = 1019.461 \pm 0.016$ MeV, the full width $\Gamma = 4.249 \pm 0.013$ MeV. In addition, there is much overlap between the ω mass region and the ρ meson mass region. Its decay mode for this peak is $\rho \to \mu\mu$. The ρ meson mass properties in PDG are: the Mass $m = 775.26 \pm 0.23$ MeV, the full width $\Gamma = 149.1 \pm 0.8$ MeV. This large width means it distributes widely. For this reason, the ρ meson can't be estimated by a mere fitting. The other compositions of this mass regions are:$\eta \to \mu\mu$, $\eta' \to \mu\mu\pi^0$ and $\omega \to \mu\mu\gamma$. Due to these complicated compositions, only three fits for the ω meson peak, ϕ meson peak and the others are adopted. First, components of "the others" are subtracted from the correlated invariant mass distribution. Hereinafter, this is called correlated background. In the previous study, this component is fitted by a quintic formula. As stated in the previous study, a polynomial function have bumps and dips, thus the ω meson peak and ϕ meson peak could be deflected. To avoid this problem, an exponential function is adopted to fit the correlated background. An exponential function decreases monotonically, thereby an exponential fit is evidently more suitable than a polynomial fit. After extracting the peaks of ω meson and ϕ meson from 0.6 to 1.2 GeV/c^2, the background is fitted from 0.5 to 1.5 region. A fitted result of correlated background is shown in Fig.22 and Fig.23

4.1.5 p_T selection

As seen in the figures of fit results, there are some difficult p_T regions to analyze. For this reason, p_T region which seems to be analyzed easily is selected. Now $2 < p_T < 3$ GeV/c region is chosen. This region can be easily seen the ω meson and the ϕ meson peaks, and has a lot of counts.

4.2 Dropping scenario

In 4.1 section, the base functions of background, ω meson peak, ϕ meson peak for simulation have been obtained. In this section, the detectability of ω meson mass modification with pole dropping scenario is evaluated. The pole dropping means that the mean mass of ω meson peak shifts to light. This scenario assumes the peak doesn't change its shape by the modification. Also, it is assumed that the hot matter is uniform temperature, so that the dropping magnitude is a certain value. A detectability evaluation with this scenario has also been researched by the previous research. The purpose that the author also study this scenario is to repeat for applying this method to other scenarios and confirm the reproducibility.
In this scenario, the invariant mass distribution is modified like Figure24.

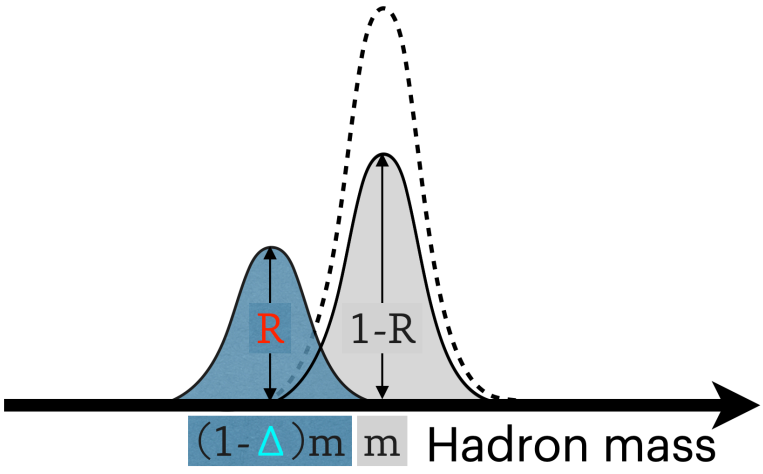

Figure 24: Conceptual drawing of ω meson mass dropping. The dot line shows ω meson mass if there were no modifications. R and Δ are the parameters which characterize dropping modification.

4.2.1 Producing mass distributions with the modification

In this section, invariant mass distributions which include ω meson mass modification with pole dropping is stated. They are produced based on the functions of background, ω meson peak and ϕ meson peak obtained in 4.1. Now, the ω meson peak function is varified. As shown in 24, ω mesons which decay in the vacuum form the normal ω meson mass peak in invariant mass distribution. On the other hand, ω mesons which deacy in the high temperature medium form the same peak shape as in the vacuum, but a different mean mass in this scenario. The mean mass is dropping, or shifting to the lighter. The dropping modification is characterized by two parameters, the ratio parameter R and the dropping magnitude parameter Δ. The R parameter means the ratio of the number of dropping ω mesons to the number of all ω mesons. The Δ parameter means how the mean mass shifts to lighter

when the original ω mass is 1.

Mass distributions with dropping ω component is created based on the background, ϕ meson, ω meson fitting functions created in section4.1. ROOT can create a histogram by shaking a random number for each bin along the function. It makes sense that random numbers fluctuate the shape of the spectrum, but it does not make sense to have different random numbers for each histogram. The results will be affected by fluctuations due to random numbers. To avoid this, a way to use same set of random numbers for all histograms is devised. First, for background and ϕ meson, which don't be modified, only one histogram with random numbers is created along the sum of their functions. For ω meson, only one histogram is created in the same way. This ω meson spectrum is divided into two parts corresponding to the parameter R, and one of them is shifted to the lighter corresponding to the parameter Δ. This method makes it possible to create all histograms from only two sets of random numbers.

4.2.2 Fitting for each R and Δ parameters

The values of the parameter R are given as 0 to 1 divided into 100 equal parts. In other words, the values of R is varied from where no ω meson modified to where all ω meson modified.

The values of the parameter Δ are given as 0 to 0.2 divided into 100 equal parts. In other words, the values of Δ are varied from where *omega* mean mass 0% dropping to where ω mean mass 20% dropping.

By the combinations of each R value and each Δ value, ten thousands histograms are created and fitted. In the result histograms, each area has a value obtained as a difference of χ^2 value of two fittings.

4.2.3 Result 1: Difference of χ^2 values in each fittings

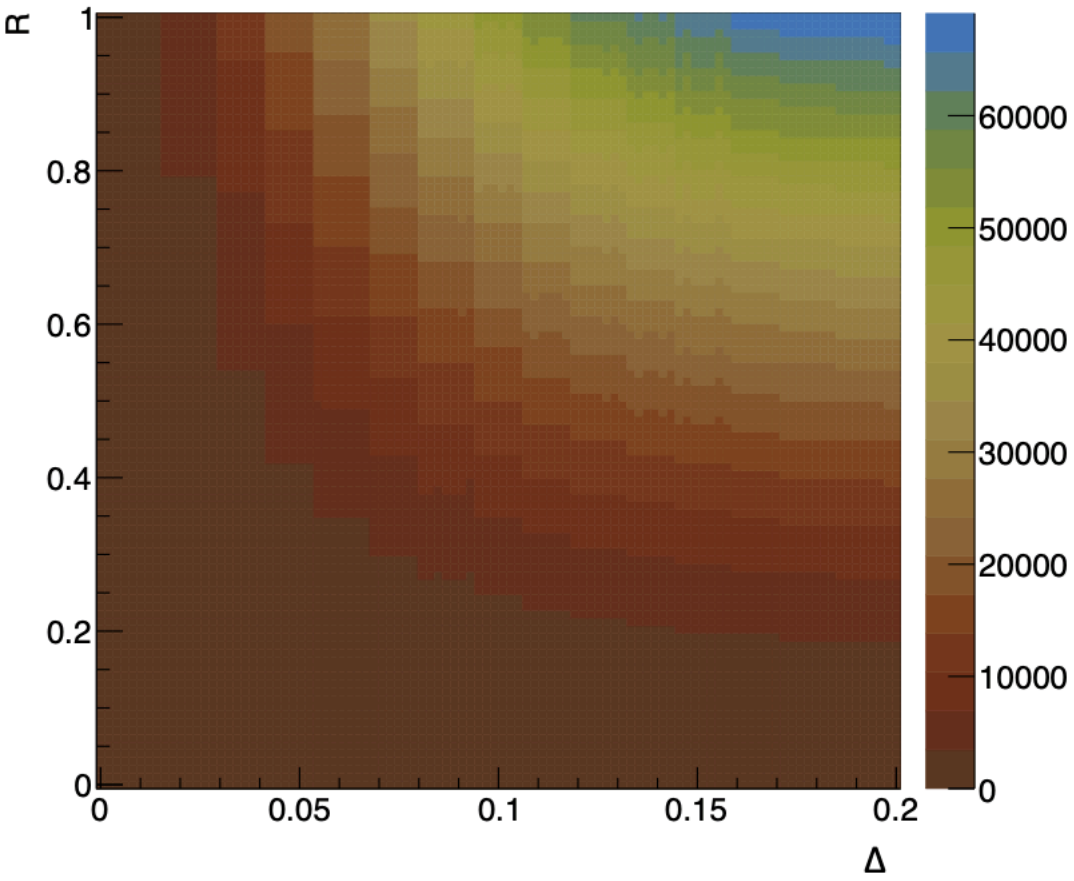

Figure 25: Detectability with ω meson pole dropping scenario (Difference of χ^2 expression)

4.2.4 Result 2: Significance expression

Fig.26 is the significance expression of the result.

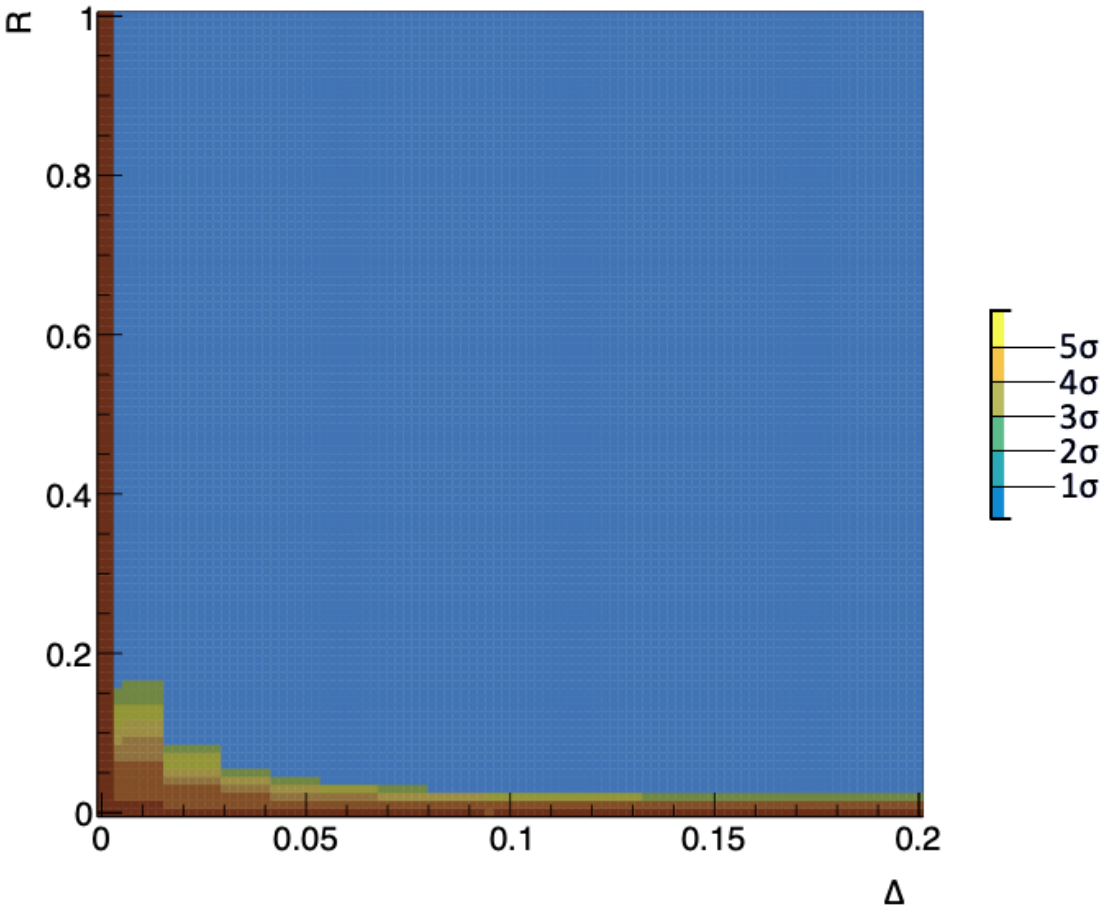

Figure 26: Detectability with ω meson pole dropping scenario (Significance expression)

4.3 Broadening scenario

In 4.1 section, the functions of background, ω meson peak, ϕ meson peak for simulation have been obtained. In this section, the detectability of ω meson mass modification with pole broadening scenario is evaluated. The pole broadening means that the width of ω meson mass peak broadens. This scenario assumes the mean mass doesn't change by the modification. Also, it is assumed that the hot matter is uniform temperature, so that the broadening magnitude is a certain value.

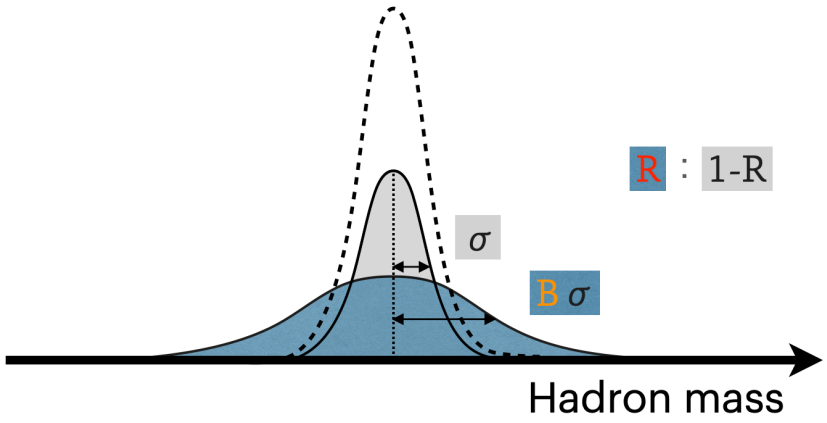

Figure 27: Conceptual drawing of ω meson mass broadening. The dot line shows ω meson mass if there were no modifications. R and B are the parameters which characterize broadening modification.

4.3.1 Producing mass distributions with the modification

In this section, invariant mass distributions which include ω meson mass modification with pole broadening is stated. They are produced based on the functions of background, ω meson peak and ϕ meson peak obtained in 4.1. Now, the ω meson peak function is varified. As shown in 27, ω mesons which decay in the vacuum form the normal ω meson mass peak in invariant mass distribution. On the other hand, ω mesons which deacy in the high temperature medium form the same mean mass, but a different peak width in this scenario. The peak width is broadening. The broadening modification is characterized by two parameters, the ratio parameter R and the broadening magnitude parameter B. The R parameter means the ratio of the number of broadening ω mesons to the number of all ω mesons. The B parameter means how the peak width broadened when the original ω peak width is 1.

Mass distributions with broadening ω component is created based on the background, ϕ meson, ω meson fitting functions created in section4.1. ROOT can create histograms with random numbers, but same as the situation of dropping scenario, it does not make sense to have different random numbers for each histogram. To avoid this problem, only a few set of random numbers

should be used for creating all histograms. However, the same way with dropping scenario is invalid. The procedure of producing histograms is as follows. First, the most broadened histogram is produced with 100 multiplied bins. Second, the most broadened histogram is shirinked corresponding to each parameter. Then, broadened ω meson histograms for each broadening parameter are obtained. In this study, this bin-merged method is adopted.

4.3.2 Fitting for each R and B parameters

The value of the parameter R is given as 0 to 1 divided into 100 equal parts. In other words, the value of R is varied from where no ω modified to where all ω modified.

The value of the parameter B is given as 1 to 3 divided into 100 equal parts. In other words, the value of B is varied from where *omega* width no broadening to where ω width 3 multiplied broadening.

By the combinations of each R value and each B value, ten thousands histograms are created and fitted. In the result histograms, each area has a value obtained as a difference of χ^2 value of two fittings.

4.3.3 Result 3: Difference of χ^2 values in each fittings

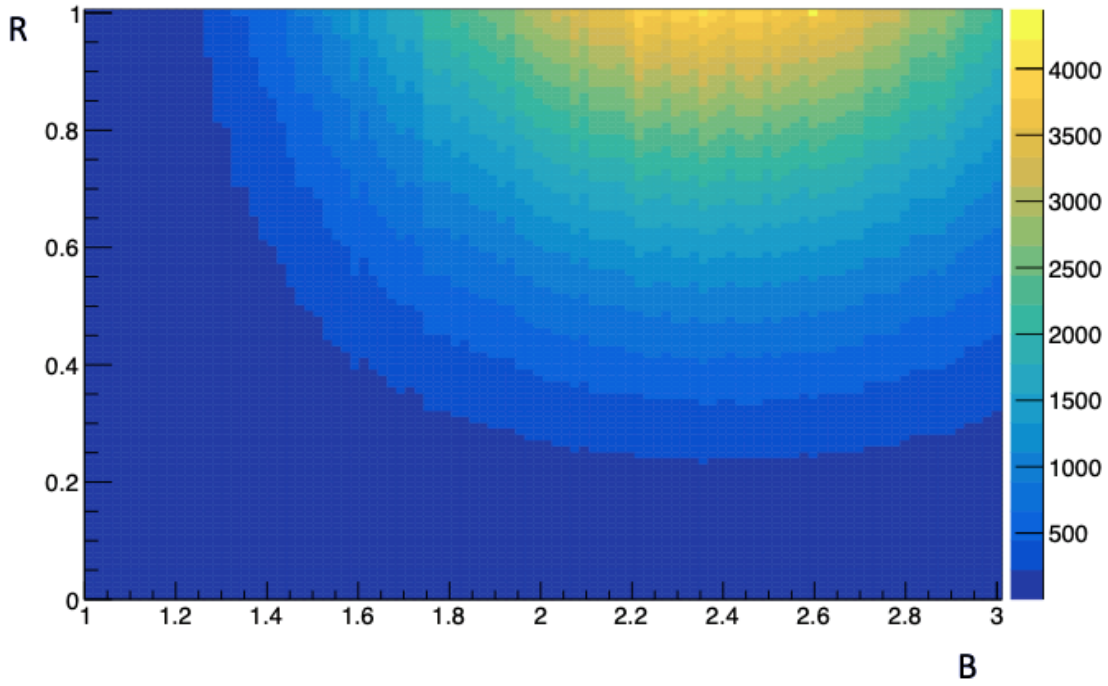

Figure 28: Detectability with ω meson pole broadening scenario (Difference of χ^2 expression)

4.3.4 Result 4: Significance expression

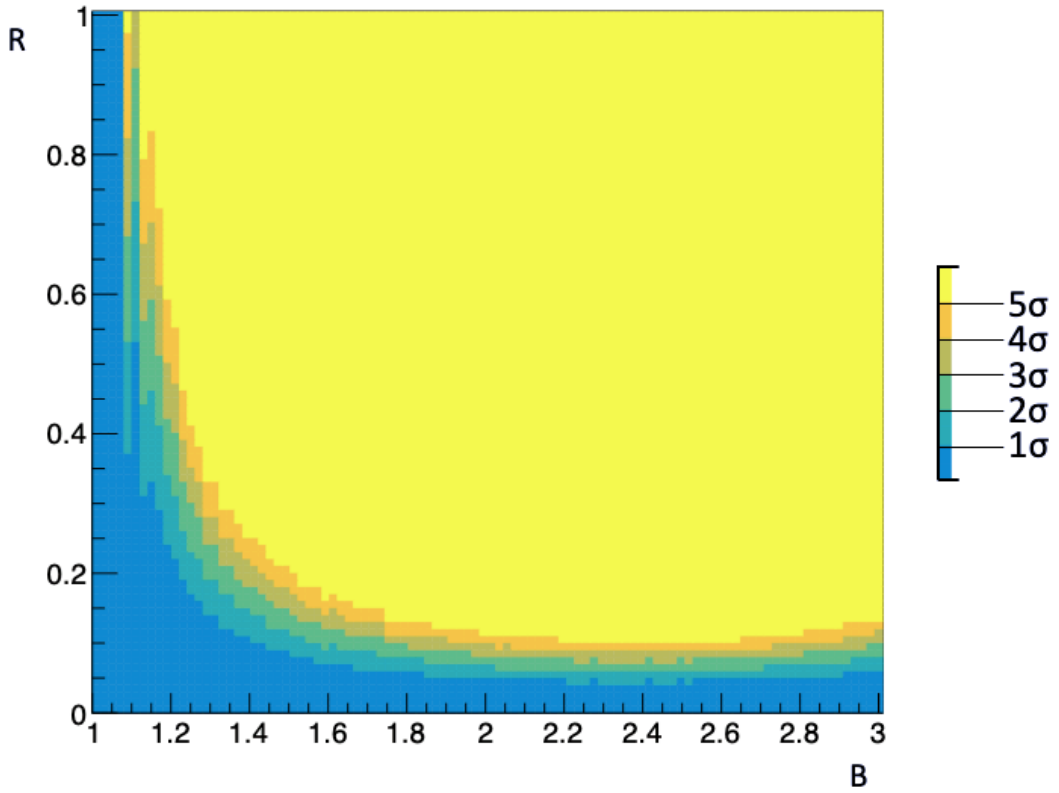

Figure 29: Detectability with ω meson pole broadening scenario (Significance expression)

4.4 Broadening and Dropping scenario

In 4.1 section, the base functions of background, ω meson peak, ϕ meson peak for simulation have been obtained. In this section, the detectability of ω meson mass modification with pole dropping and broadening scenario is evaluated. The pole of ω meson peak shifts to light. Moreover, the mass width broadens. Also, it is assumed that the hot matter is uniform temperature, so that the dropping magnitude and broadening magnitude are certain values, respectively.
Previous study assumes omega meson's mass dropping, and This study assumes omega meson's mass broadening. Actually, both of these mass modification should appear simultaneously. Hence, it is worthwhile to consider a scenario where these two modifications happen as the same time. Consequently, This 'double' modification model should be assumed. This modification scenario is modeled with three parameters, the dropping parameter Δ, the broadening parameter B and the proportion parameter R. The method to this scenario is referred the strategy of the broadening scenario. Based on a broadening histogram, histograms corresponding to each Δ and R parameters, are produced. By this procedure, only a set of random numbers is used. Due to this, the fluctuations of random numbers are suppressed.

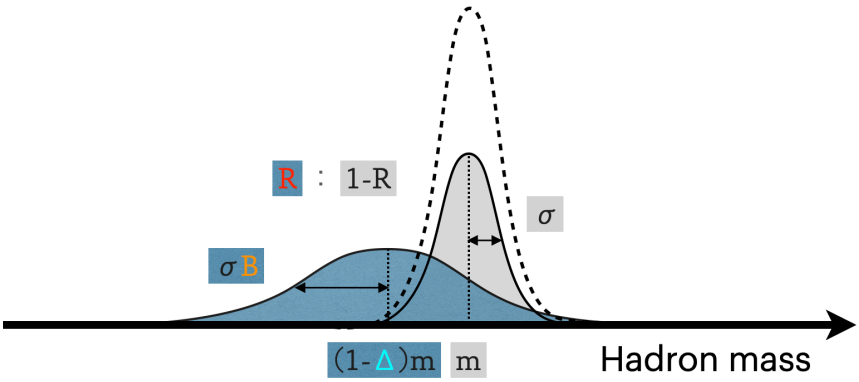

Figure 30: Conceptual drawing of ω meson mass dropping and broadening. The dot line shows ω meson mass if there were no modifications. R, Δ and B are the parameters which characterize dropping modification.

In this scenario, the invariant mass distribution is modified like Figure30.

4.4.1 Producing mass distributions with the modification

In this section, invariant mass distributions which include ω meson mass modification with pole dropping and broadening is stated. They are produced based on the functions of background, ω meson peak and ϕ meson peak obtained in 4.1. Now, the ω meson peak function is varified. As shown in 30, ω mesons which decay in the vacuum form the normal ω meson mass peak

in invariant mass distribution. On the other hand, ω mesons which deacy in the high temperature medium form the broadening peak compared to it in a vacuum, and a lighter mean mass in this scenario. The dropping and broadening modification is characterized by three parameters, the ratio parameter R and the dropping magnitude parameter Δ and the broadening magnitude parameter B. The R parameter means the ratio of the number of dropping ω mesons to the number of all ω mesons. The Δ parameter means how the mean mass shifts to lighter when the original ω mass is 1. The B parameter means how the peak width broadened when the original ω peak width is 1.

4.4.2 Producing mass distributions with the modification

In this section, invariant mass distributions which include ω meson mass modification with pole broadening is stated. They are produced based on the functions of background, ω meson peak and ϕ meson peak obtained in 4.1. Now, the ω meson peak function is varified. As shown in 27, ω mesons which decay in the vacuum form the normal ω meson mass peak in invariant mass distribution. On the other hand, ω mesons which deacy in the high temperature medium form the same mean mass, but a different peak width in this scenario. The peak width is broadening. The broadening modification is characterized by two parameters, the ratio parameter R and the broadening magnitude parameter B. The R parameter means the ratio of the number of broadening ω mesons to the number of all ω mesons. The B parameter means how the peak width broadened when the original ω peak width is 1.

Mass distributions with broadening ω component is created based on the background, ϕ meson, ω meson fitting functions created in section4.1. ROOT can create histograms with random numbers, but same as the situation of dropping scenario, it does not make sense to have different random numbers for each histogram. To avoid this problem, only a few set of random numbers should be used for creating all histograms. However, the same way with dropping scenario is invalid. The procedure of producing histograms is as follows. First, the most broadened histogram is produced with 100 multiplied bins. Second, the most broadened histogram is shirinked corresponding to each parameter. Then, broadened ω meson histograms for each broadening parameter are obtained. In this study, this bin-merged method is adopted.

4.4.3 Fitting for each R, Δ and B parameters

The value of the parameter R is given as 0 to 1 divided into 10 equal parts. In other words, the value of R is varied from where no ω modified to where all ω modified.

The values of the parameter Δ are given as 0 to 0.2 divided into 100 equal parts. In other words, the values of Δ are varied from where *omega* mean mass 0% dropping to where ω mean mass 20% dropping.

The value of the parameter B is given as 1 to 3 divided into 100 equal parts. In other words, the value of B is varied from where *omega* width no

broadening to where ω width 3 multiplied broadening.

By the combinations of each R value and each Δ value and B value, one hundred thousand histograms are created and fitted. In the result histograms, each area has a value obtained as a difference of χ^2 value of two fittings.

4.4.4 Result 5: Difference of χ^2 values in each fittings

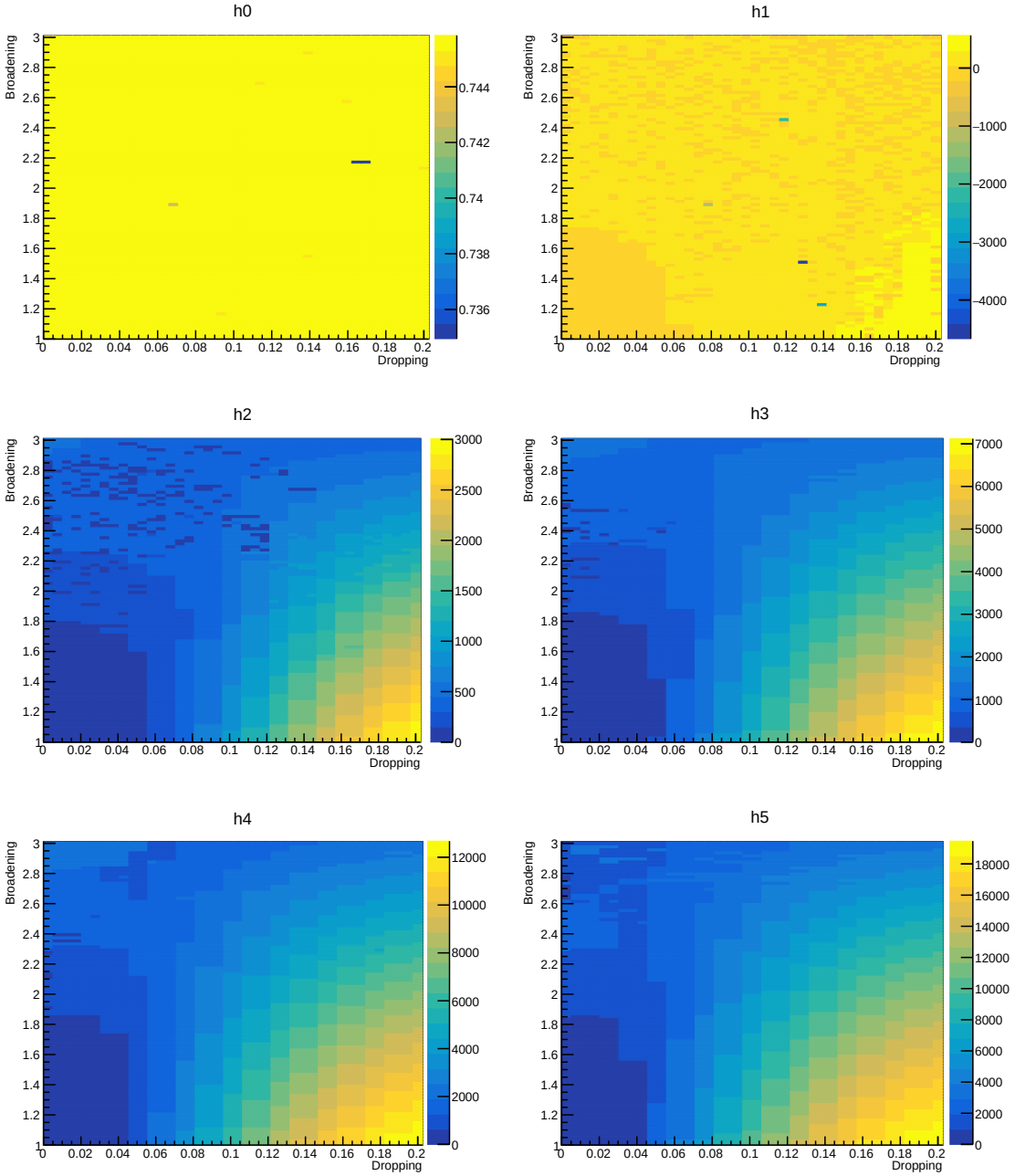

Figure 31: Detectability with ω meson pole dropping and broadening scenario (Difference of χ^2 expression)

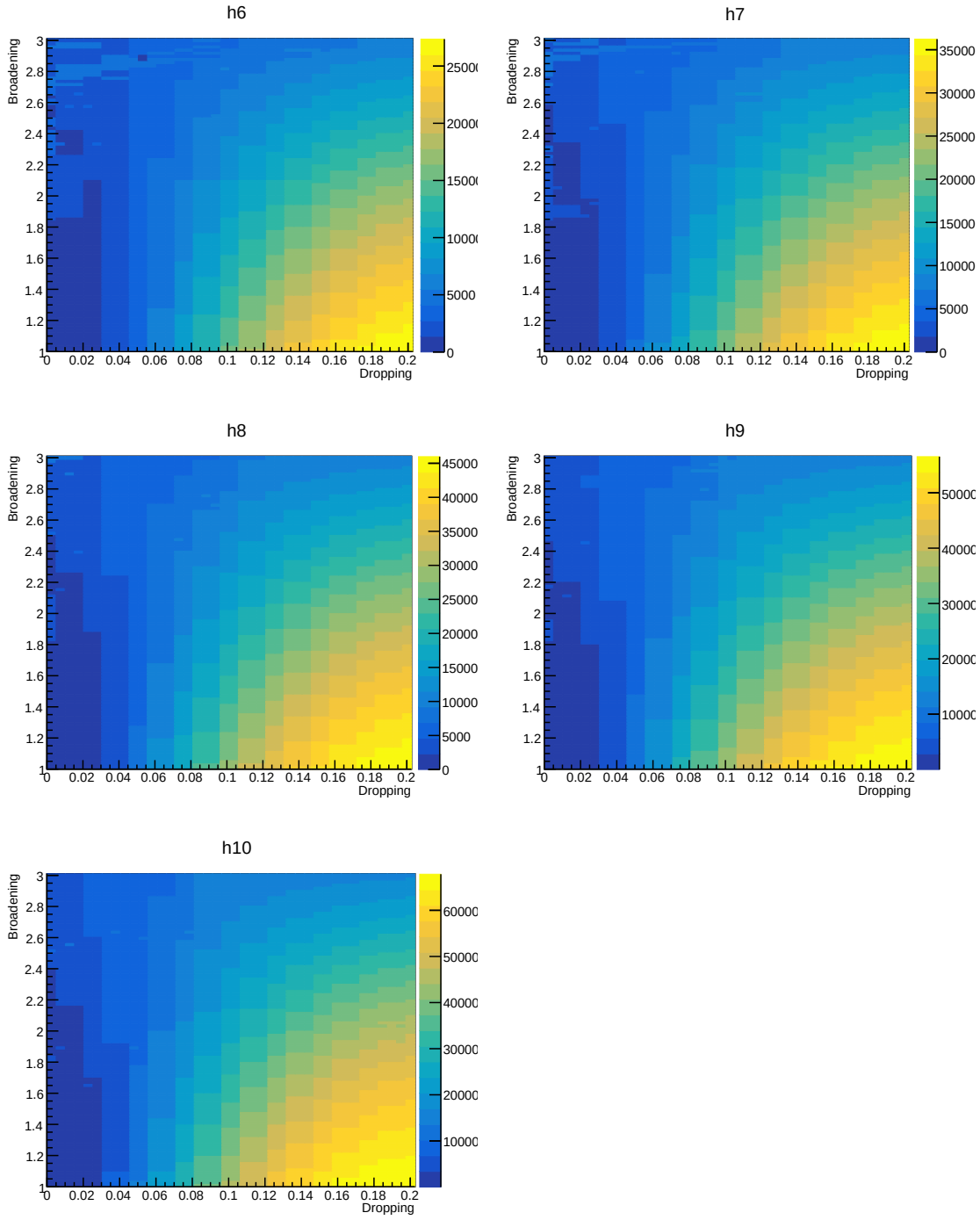

Figure 32: Detectability with ω meson pole dropping and broadening scenario (Difference of χ^2 expression)

4.4.5 Result 6: Significance expression

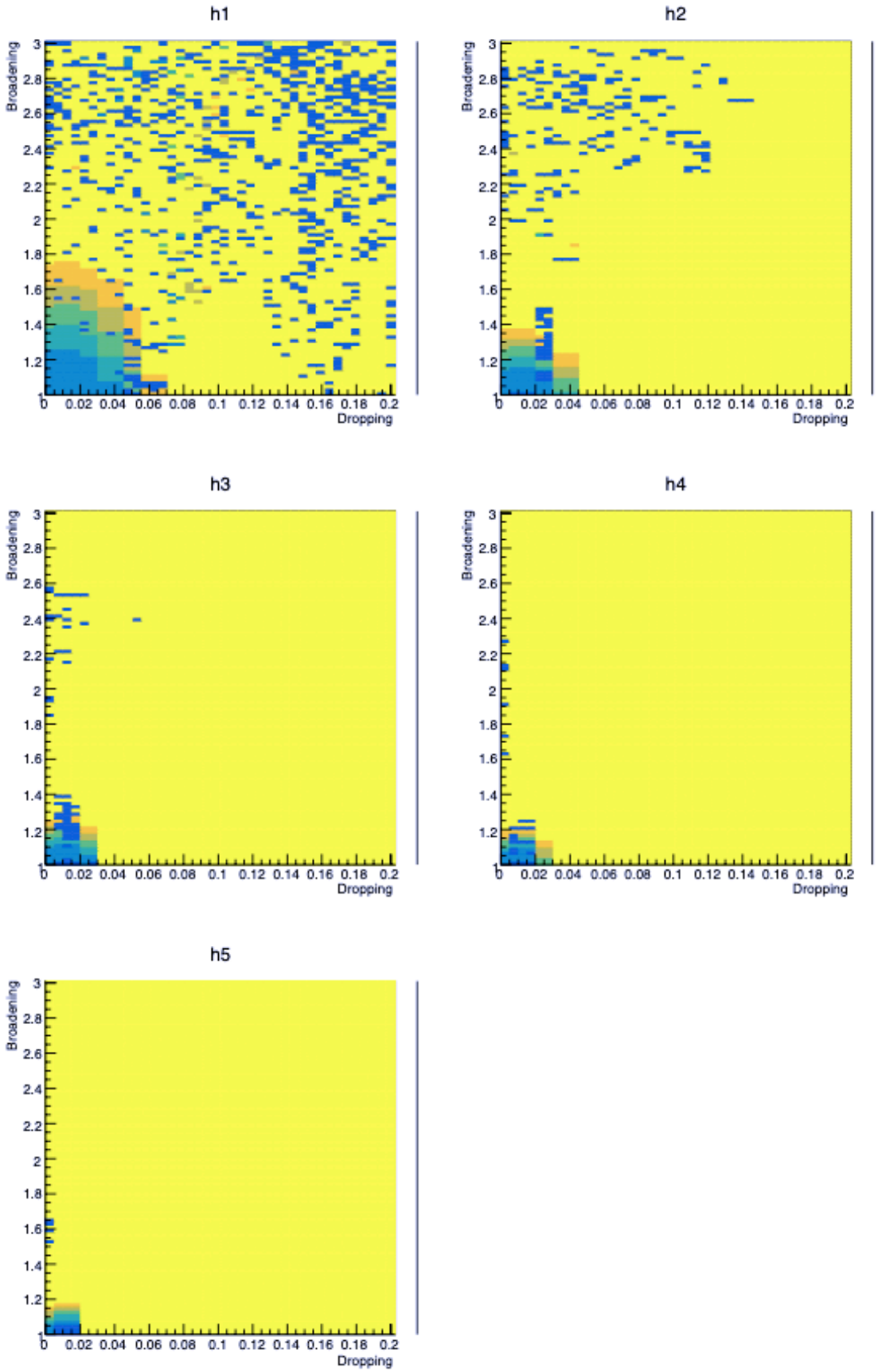

Figure 33: Detectability with ω meson pole dropping and broadening scenario (Significance expression)

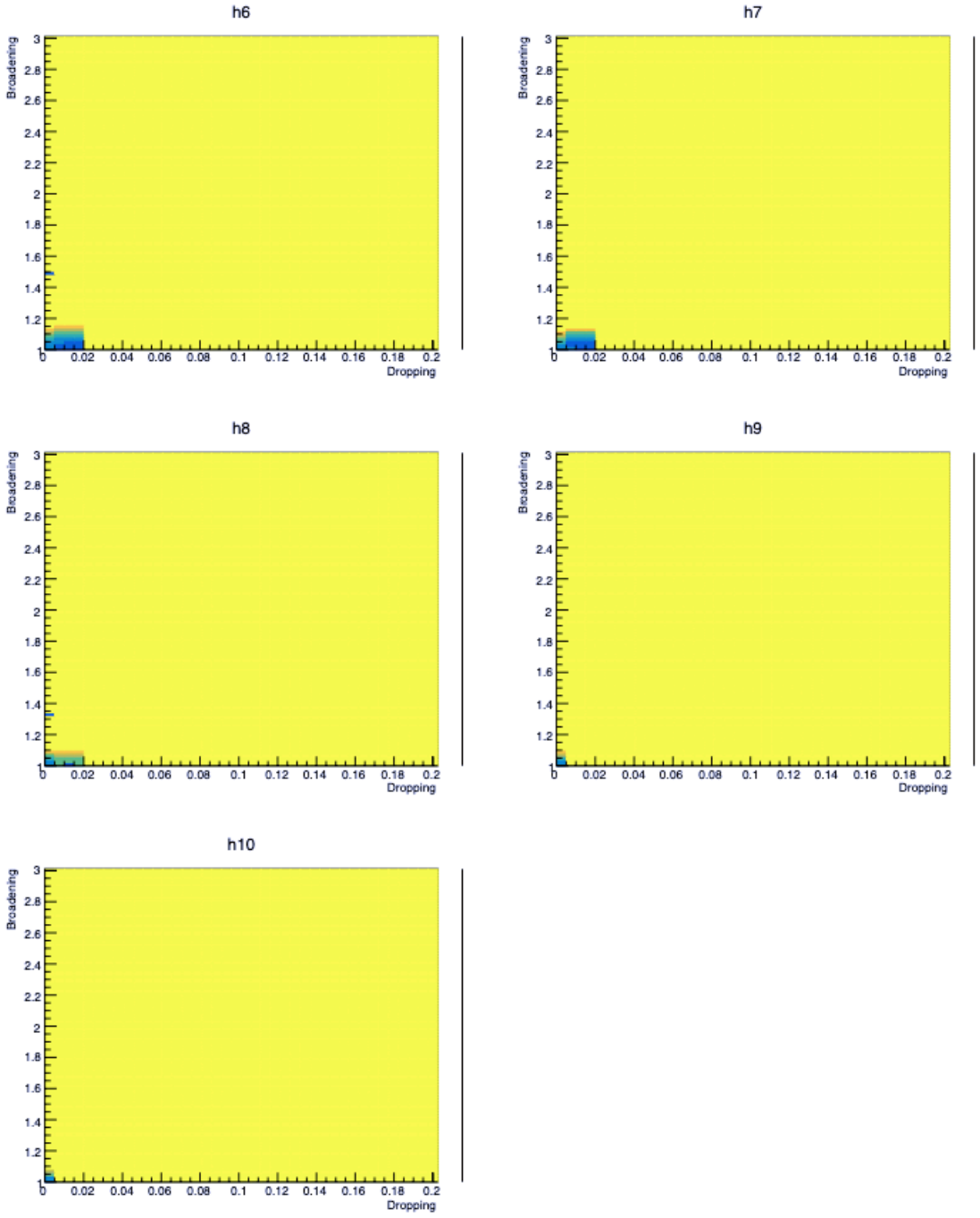

Figure 34: Detectability with ω meson pole dropping and broadening scenario (Significance expression)

5 Discussion

The result of detectability with pole mass dropping is shown in Fig. 25 and Fig. 26. Based on the results, the higher the R value, the higher detectability, and the higher the Δ value, the higher detectability. Typically, if there is 10% of ω meson mean mass dropping, the mass modification can be seen.

The result of detectability with pole width broadening is shown in Fig. 29 and Fig. **??**. Based on the results, the higher the R value, the higher detectability, and the higher the B value, the higher detectability. Typically, if there is 30% of ω meson width broadening 1.5 times, the mass modification can be seen.

The result of detectability with pole mass dropping and width broadeningc is shown in Fig. 31, Fig. 32, Fig. 33 and Fig. 34. Based on the results, the higher the R value, the higher detectability, and the higher the Δ value, the higher detectability. When Δ is under a few percents, the higher the B value, the higher detectability. When Δ is over a few percents, the lower the B value, the higher detectability. Typically, if there is 50% of ω mean mass 5% dropping and width broadening 1.5 times, the mass modification can be seen. Although, the results in this study are obtained with the following problems:

1) The background have been subtracted by exponential. Although it is no longer an arbitrary fit than the 5th order fit in the previous study, it is better to be subtract by the estimation obtained by simulation using event generator.

2) The mass change due to partial restoration of the chiral symmetry is a function of temperature. Since the temperature is not uniform in the QGP, the degree of change in the mass state should vary depending on at which space-time point the meson decays. In this case, however, the results are based on the assumption that the temperature is uniform with respect to all ω mesons.

3) When assuming a change in the mass state of ω, there are no reasons not to assume that the mass states of ρ and ϕ mesons, which are also light vector mesons, are changing. However, this time we only assume a mass change of ω. The detectability of the mass state change may differ greatly depending on the mass modification of other mesons.

4) There is a possibility that ω meson may overlap and interfere when the ϕ meson has mass dropping or broadening. Of course, ω could also live without overlapping if dropped, but we cannot discuss the result in the case which ϕ changes at the same time and overlaps to ω meson.

6 Conclusion

The study of detectability of ω meson mass modification with pole dropping and/or broadening scenarios was conducted, as a preliminary feasibility study for analyzing light vector mesons' mass modification in QGP produced by Pb-Pb collisions in Run 3 at ALICE.

This study derived the numerical result of detectability when the ω meson mass drops and/or broadens. And the evaluation method for pole dropping and/or broadening was established. This method can be applied not only to ω meson, but also other mesons, such as ρ meson and ϕ meson. This method is useful for more advanced detectability evaluation, such as scenarios including temperature parameter. This is a simulation based on the data samples of pp collisions in Run 2. Toward the analysis of mass modification in Pb-Pb collisions in Run 3, from now on, the Pb-Pb data is used for this evaluation. Additionally, the background estimation by event generator and ϕ and ρ meson modification simultaneously is the way to improve the evaluation. Moreover, the other selection like multiplicity and so on should be tried. The analysis for Pb-Pb is more difficult due to the amount of background.
Therefore, it is necessary to improve simulation and analysis for discovering restoration of chiral symmetry in Pb-Pb collisions in Run 3 at ALICE.

7 Acknowledgements

First of all, I would like to express my appreciation to my supervisor, Prof. Kenta Shigaki. His support for my research was essential and he gave me a prime contribution for finishing my master's course. I owe entirely him that I was able to come this far. I cannot thank him enough.

I am sincerely grateful to Assoc. Prof. Yorito Yamaguchi. He cared and tried to support me a lot. He taught me a lot of basics of being a researcher. He always told me what I was missing in myself and my research.

I am deeply grateful to Assis. Prof. Satoshi Yano. He gave me a lot of beneficial advices and supports for my research and conference presentation.

Assco. Prof. Kensuke Homma and Assis. Prof. Takahiro Miyoshi gave me a lot of assistances to understand physics. Mr. Masanori Ogino gave me helpful advices. I appreciate Prof. Chikako Moriyoshi being my mentor. Mr. Kazami Yamamoto, Japan Atomic Energy Agency, gave me a valuable opportunity to study at J-PARC.

I am grateful to Mr. T. Kondo who gave me a lot of support to begin my research. I appreciate Mr. Ueda, Mr. Yamakawa, Mr. Osako, Mr. Oya, Mr. Kirita and Ms. Shibata for helping me as seniors of the Lab. I also thank to all the colleagues of Quark Physics Lab. for being friendly. Especially, I thank Fumiya Ishibashi and Sigekuni Sotaro for experiencing the Labex and the seminor together. Special thanks to R. E. for sharing various things. I am especially grateful to Kento Kimura and Ryoka Tokumoto for sharing research life with me.

I would like to thank all the other people who have been involved in my study.

Finally, I would like to appreciate to my family for supporting my life.

References

[1] Gauss Centre for Supercomputing. Numerical Determination of the Phase Diagram of Nuclear Matter.

[2] W. Weise. Nuclear aspects of chiral symmetry. *Nuclear Physics A*, 1993.

[3] X. Zhu et al. DD correlations as a sensitive probe for thermalization in high energy nuclear collisions. *Physics Letter B*.

[4] Tapan K. Nayak. Heavy ions: Results from the Large Hadron Collider. *Pramana – Journal of Physics*, 2012.

[5] E. Lopienska. The CERN accelerator complex, layout in 2022, 2022.

[6] The ALICE Collaboration et al. The ALICE experiment at the CERN LHC. *Journal of Instrumentation*, 2008.

[7] Raphael Tieulent. Muon forward tracker status. *12th ALICE ITS Upgrade, MFT,and O2 Asian Workshop*, 2018.

[8] The ATLAS Collaboration. Observation of a new particle in the search for the Standard Model Higgs boson with the ATLAS detector at the LHC.

[9] The CMS Collaboration. Observation of a new boson at a mass of 125 GeV with the CMS experiment at the LHC.

[10] O. Brüning, P. Collier, P. Lebrun, S. Myers, R. Ostojic, J. Poole, and P. Proudlock. LHC Design Report Volume.1 : the LHC Main Ring, 2004.

[11] O. Brüning, P. Collier, P. Lebrun, S. Myers, R. Ostojic, J. Poole, and P. Proudlock. LHC Design Report Volume.2 : the LHC Infrastructure and General Services, 2004.

[12] M. Benedikt, P. Collier, V. Mertens, J. Poole, and K. Schindl. LHC Design Report Volume.3 : the LHC Injector Chain.

[13] K. Adcox et al.

[14] Ryugo S. Hayano and Tetsuo Hatsuda. Hadron properties in the nuclear medium. *Rev. Mod. Phys.*, 2010.

[15] ALICE Collaboration. Performance of the ALICE Experiment at the CERN LHC, 2014.

[16] et al. F. Orsini. Conceptual design of the Muon Forward Tracker of the ALICE experiment. *IEEE Transactions on Nuclear Science*, 2012.

[17] Y. Nambu and journal=Phys. Rev. year=1961 G. Jona-Lasinio, title=Dynamical model of elementary particles based on an analogy with superconductivity. I.

[18] Y. Nambu and journal=Phys. Rev. year=1961 G. Jona-Lasinio, title=Dynamical model of elementary particles based on an analogy with superconductivity. II.

[19] P. Higgs. Broken Symmetries and the Mases of Gauge Bosons. *Physical Review Letters*, 1964.

[20] F. Enclert and R. Brout. Broken Symmetry and the Mass of Gauge Vector Mesons. *Physics Revier Letters*, 1964.

[21] Carl Richard Hagen, Thomas Wlter Bannerman Kibble, and Gerald Guralnik.

[22] title=NA60 results on the ρ spectral function in In-In collisionsm journal=Nuclear Physics A year=2007 S. Damjanovic, the NA60 Collaboration.

[23] Ryugo S. Hayano and journal=Rev. Mod. Phys. year=2010 Tetsuo Hatsuda, title=Hadron properties in the nuclear medium.

[24] ALICE collaboration. Addendum of the Letter of Intent for the upgrade of the ALICE experiment : The Muon Forward Tracker. *CERN-LHCC-2013-014 ; LHCC-I-022-ADD-1*, 2013.

[25] ALICE collaboration. Technical Design Report for the Muon Forward Tracker. *CERN-LHCC-2015-001 ; ALICE-TDR-018*, 2015.

[26] T. Kondo. Detection feasibility evaluation with a two-level model of mass spectra modification of light vector mesons, 2019.

[27] P. Crochet and P. Braun. Investigation of background subtraction techniques for high mass dilepton physics. *Nuclear Instruments and Methods in Physics Research A*, 2002.